

1-1-2008

On the use of fiber optic sensors embedded in fiber reinforced polymers

Lesha Kolubinski
Ryerson University

Follow this and additional works at: <http://digitalcommons.ryerson.ca/dissertations>



Part of the [Aerospace Engineering Commons](#)

Recommended Citation

Kolubinski, Lesha, "On the use of fiber optic sensors embedded in fiber reinforced polymers" (2008). *Theses and dissertations*. Paper 955.

**ON THE USE OF FIBER OPTIC SENSORS EMBEDDED IN
FIBER REINFORCED POLYMERS**

by

Lesha Kolubinski

Bachelor of Aerospace Engineering

Ryerson University, 2006

A thesis

presented to Ryerson University

in partial fulfillment of the
requirements for the degree of
Masters of Applied Science
in the Program of
Aerospace Engineering

Toronto, Ontario, Canada, 2008

© (Lesha Kolubinski) 2008

Author's Declaration

I hereby declare that I am the sole author of this thesis.

I authorize Ryerson University to lend this thesis to other institutions or individuals for the purpose of scholarly research.

Signature

I further authorize Ryerson University to reproduce this thesis by photocopying or by other means, in total or in part, at the request of other institutions or individuals for the purpose of scholarly research.

Signature

Borrower's Page

Ryerson University requires the signatures of all persons using or photocopying this thesis. Please sign below, and give the address and date.

NAME	SIGNATURE	ADDRESS	DATE

Acknowledgements

The author would like to acknowledge and thank her professors for the opportunity and for their support; Dr. C. Poon, Dr. Z. Fawaz and Dr. K. Behdinan.

This work was done with the assistance of Dr. X. Gu of the Optical Research Laboratory in the Department of Electrical Engineering of Ryerson University. Dr. X. Gu aided with providing the fiber optic sensors used in this research.

The specimens used in this research were fabricated with the assistance of Dr. Hamada, Dr. Nakai, Y. Takai and S. Tomohiko with the Advance Fibro Science Department at the Kyoto Institute of Technology in Kyoto Japan.

In addition to those mentioned above, the author would like to especially thank her parents, Al and Rose Kolubinski, for their undying encouragement, love and support.

ON THE USE OF FIBER OPTIC SENSORS EMBEDDED IN FIBER REINFORCED POLYMERS

**Lesha Kolubinski – Ryerson University, Toronto
Masters of Applied Science – Aerospace Engineering – 2008**

Abstract

Smart structures and structural health monitoring are advancing fields that have potential to yield many benefits to many industries and applications. It is important for applicable sensing technologies to mature so that they may be relied upon. Fiber optic sensors are one such sensing method. Their use in fiber reinforced polymer, FRP, composite materials is reviewed and examined, specifically embedded fiber optic sensors. A fabrication method for embedding fiber Bragg grating, FBG, fiber optic sensors in FRP specimens was developed. This fabrication method is then validated through mechanical testing. Initial specimen stiffness's were determined and the results from the FBGs compared well with mechanical resistance strain gauges. The FBG sensors were also successful in detecting drops in stiffness of the specimens when subjected to fatigue loading.

Table of Contents

Author’s Declaration.....	ii
Borrower’s Page.....	iii
Acknowledgements.....	iv
Abstract.....	v
Table of Contents.....	vi
Table of Figures.....	viii
List of Tables.....	x
List of Symbols.....	xi
Scope and Objective.....	1
1 Introduction.....	3
1.1 Smart Materials and Structures.....	3
1.2 Structural Health Monitoring.....	4
2 Composite Materials.....	6
2.1 Introduction.....	6
2.2 Manufacturing Methods.....	6
2.2.1 Wet Hand Lay Up Procedure.....	6
2.3 Residual Stress.....	7
2.4 Mechanical Properties.....	9
2.5 Fatigue Behavior.....	11
3 Fiber Optic Sensors.....	13
3.1 Introduction.....	13
3.2 Principle of Operation.....	13
3.3 Fiber Bragg Grating.....	16
3.4 Other Types of Fiber Optic Sensors.....	21
4 Internal Monitoring of FRPs with Embedded Fiber Optic Sensors.....	23
4.1 Material Fabrication.....	23
4.2 Specimen Testing.....	24
4.2.1 Fatigue Testing.....	26

5	Specimen Fabrication.....	28
5.1	Preliminary Specimens	28
5.1.1	Fiber Placement Experimentation.....	28
5.1.2	First Specimen	31
5.1.3	Second Specimen	32
5.2	Clay Method Procedure	35
5.2.1	Pre-cure	35
5.2.2	Post-cure	40
5.3	Fabrication Method Summary	42
5.4	Specimen Summary	43
6	Experimentation.....	46
6.1	Sensor Selection.....	46
6.1.1	Mechanical Resistance Strain Gauges	46
6.1.2	Fiber Bragg Grating Sensors.....	49
6.2	Sensor Calibration.....	49
6.2.1	Beam Bending.....	50
6.2.2	Tensile Specimen	54
6.3	Embedded Fiber	57
6.3.1	Wavelength Spectrums	57
6.3.2	Residual Stress evaluation	60
6.4	Tensile Testing.....	60
6.5	Fatigue Testing.....	65
6.5.1	Preliminary Testing.....	66
6.5.2	Low Cycle Fatigue.....	69
6.5.3	High Cycle Fatigue	73
6.6	Further Discussion	76
	Conclusion	78
	References.....	79

Table of Figures

Figure 1 - Venn Diagram [1]	3
Figure 2 - Isochromatic Fringes of a Transversely Loaded Unidirectional Composite....	10
Figure 3 - Law of Refraction	14
Figure 4 - Core and Cladding.....	15
Figure 5 - Anatomy of a Fiber Optic	15
Figure 6 - Fiber Optic Multiplexing	16
Figure 7 – Perturbations of the Refractive Index.....	17
Figure 8 - Sensing Concept of FBGs [19]	18
Figure 9 - Standard Setup	18
Figure 10 - Periodic Change in Index of Refraction.....	20
Figure 11 - Chirped Grating.....	21
Figure 12 – Panda and Bow-tie fibers.....	22
Figure 13 - First Fiber Optic Array Layout	29
Figure 14 - Glue Trial Specimens.....	30
Figure 15 - Glue Trial Specimens a) Cyanoacrylate b) Rapid Cure Epoxy and c) Standard Epoxy	31
Figure 16 - First Specimen with Damaged Fiber Optic.....	32
Figure 17 - Specimen Constructed using Reduced Resin Method and Clay Method.....	33
Figure 18 - Fiber Optic Damaged with Reduced Resin Method	34
Figure 19 - Fiber Optic Intact with Clay Method	35
Figure 20 - Protective Tubing Affixed to Fabric	36
Figure 21 - Fabric with Fiber Optics in Place.....	37
Figure 22 - Bottom Fabric Layer with Fiber Optics in Place	38
Figure 23 - Impregnation of Bottom Fabric Layers with Exposed Fiber Optics	39
Figure 24 - Excess Resin and Fiber Exit Pre-cure	40
Figure 25 - Brittle Clay Post-cure.....	40
Figure 26 - Undamaged Fiber Optics Post-cure	41
Figure 27 - Removal of Excess Resin and Specimen Cutting Post-cure	42
Figure 28 - Desired Specimen Layout	43

Figure 29 - Specimen Design.....	44
Figure 30 - End of Specimen to be Clamped.....	45
Figure 31 - Fiber Optic Array Layout.....	49
Figure 32 - Beam Bending Calibration Specimen.....	51
Figure 33 - Beam Bending Calibration Setup.....	52
Figure 34 - FBG Calibration Curve (Beam Bending).....	53
Figure 35 - FBG Calibration Factor (Beam Bending).....	54
Figure 36 - Gauges Strain Readings with Respect to Time.....	55
Figure 37 - Tensile Specimen.....	56
Figure 38 - Debonded Strain Gauges.....	57
Figure 39 - Change in Reflected Wavelengths of Embedded Fiber Optic Array.....	58
Figure 40 - Freestate and Embedded Spectrums with Same Reference Line.....	59
Figure 41 - Test Setup.....	61
Figure 42 - Spectrum Changes During Loading.....	62
Figure 43 - Highly Chirped Spectrum.....	64
Figure 44 - Damage Accumulation from Initial Loading.....	65
Figure 45 - Preliminary Specimens.....	66
Figure 46 - Preliminary Fatigue Specimen.....	67
Figure 47 - Preliminary Specimen Damage Accumulation.....	68
Figure 48 - Cracks in Strain Gauge.....	68
Figure 49 - Drop in Modulus.....	70
Figure 50 - Percent Drop in Stiffness.....	71
Figure 51 - Delamination Buckling.....	72
Figure 52 - After Specimen Fracture.....	73
Figure 53 - Portion of Entire Light Spectrum Reflected.....	74
Figure 54 - Zero Load Reflection Spectrum.....	75
Figure 55 - Specimen Longitudinal Cross Section.....	76

List of Tables

Table 1 – Mechanical Properties from Previous Testing.....	45
Table 2 - Specimen Residual Strains	60
Table 3 - Initial Specimen Moduli	63

List of Symbols

E	Youngs Modulus
F	Force
I	Moment of Inertia or Electrical Current
L	Length
P	Power
V	Voltage
c	Distance from Neutral Axis
d	Distance from Applied Force
dB	Decibel
n	Index of Refraction
n_e	Effective Index of Refraction
nm	Nanometer
nW	Nanowatt
t	Thickness
w	Width
Ω	Ohm
Λ	Pitch
θ	Angle of Incidence
δ	Displacement
ε	Strain
λ	Wavelength
ν	Poissons Ratio
$\mu\varepsilon$	Microstrain

Scope and Objective

This thesis was conducted in collaboration with Ryerson University's Department of Aerospace Engineering and The Kyoto Institute of Technology's Advanced Fibro Science Department, in Kyoto Japan. The Facility for Research on Aerospace Materials and Engineered Structures (F.R.A.M.E.S.), within the Department of Aerospace Engineering at Ryerson University, and the author of this thesis remained the main organizer(s) and focal point throughout this research endeavor. These collaborations were formed based on mutual interest in investigating embedding methods and/or internal measurement capabilities of embedded fiber optic sensors, specifically fiber Bragg grating sensors, FBGs, within fiber reinforced polymer, FRP, specimens.

Fiber optic sensors were fabricated and provided by the Optical Research Laboratory, within the Department of Electrical Engineering at Ryerson University. The sensors were then taken, by the author, to the Advanced Fibro Science Department in Kyoto Japan. In Kyoto it was desired to formulate and develop a reliable and repeatable method for embedding the fiber optic sensors into FRP specimens utilizing the equipment and techniques made available there. With a successful method developed, a number of specimens of various types were then to be fabricated with the fiber optic sensors embedded within the material. Further measurements and testing would then be required to further validate the embedding processes.

Readings taken from the sensors both before and after embedment could then be compared with research published by other researchers to help determine validity of the processes, along with comparison and analysis of the results determined by mechanical testing. With the process validated, i.e. proof that the embedded sensor can be used to record meaningful data, further investigation into applicable application of the embedded sensors is then possible.

Due to the complex nature of FRP fatigue behavior and fatigue life determination, it was desired to investigate the appropriateness of the use of the embedded FBG sensors to

determine fatigue damage in the form of a stiffness drop of the material. This and all other mechanical testing was conducted within the F.R.A.M.E.S. laboratory of Ryerson University's Department of Aerospace Engineering. Further, due to the current developmental nature of the uses and applications of embedded FBG sensors, the results of the fatigue testing experiments would be considered important and worthwhile findings regardless of the sensors ability to detect a drop in stiffness of the specimen.

1 Introduction

1.1 Smart Materials and Structures

Smart materials and smart structures are vague terms that can be used to describe a variety of ideas. These terms often appear to be interchangeable between any sort of material or structure that is capable of more than its primary purpose. This can include compensating capabilities often tied into sensing capabilities. Often, the term is used based on a material or structures additional sensing capability alone. In his book R. Measures [1] makes use of Figure 1 when discussing smart structures.

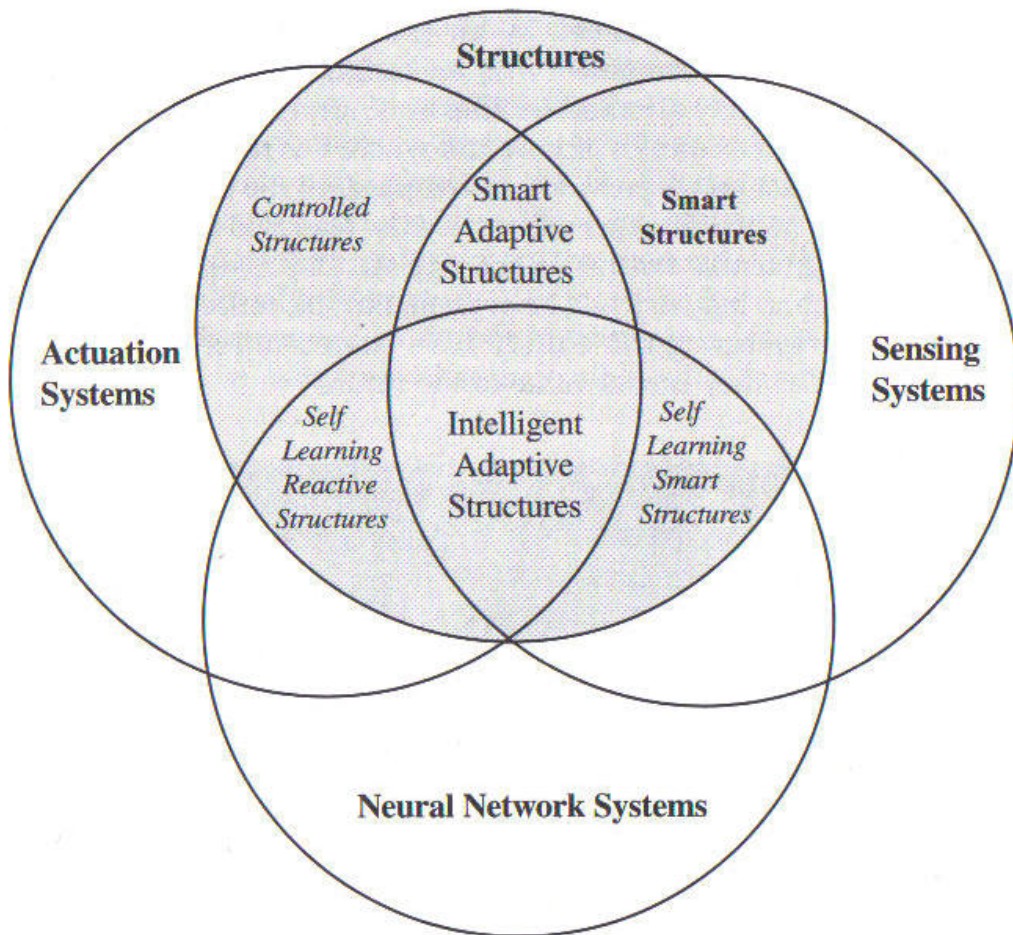


Figure 1 - Venn Diagram [1]

As can be seen, sensing systems play a vital role in the development of smart structures. Not only does the sensing system itself need to be mature and reliable but also its interaction with the structure. That is to say that the sensing system must be compatible with the structure. Although it may be most desirable to have a structure and sensing system that can interact with each other and not affect each other, this may not be possible. In such an instance where one has an effect on the other, this effect must be thoroughly understood and accounted for. Any diminishing effects should be as minimal as possible. This is not only the case for the smart structure initially but throughout the course of its lifetime.

A lot of excitement and enthusiasm has developed over the concepts of smart structures and adaptive structures. Should a structure with an integrated sensing system be coupled with adaptive capabilities then structures that can alter their shape to achieve desired behaviors can result. An example of this is a wing that can optimize its airfoil shape depending on airspeed to achieve maximum lift at that speed or phase of flight. This is one example of many desired designs that have yet to be matured and is a complex task indeed. For such structures to mature the underlying systems must have matured, as well as their integration.

1.2 Structural Health Monitoring

There are many benefits to monitoring the health of a structure. These may include lower inspection/maintenance costs for a structure, unforeseeable damage detection and hence increased safety and also residual life or replacement life estimates. In its essence, structural health monitoring entails a passive sensing system that can provide information on the integrity of the structure. This could include strain, temperature, corrosion or any other specific factor of concern should the sensing capabilities exist.

Of particular interest in the aerospace industry is damage detection and load history. Structural inspections are a costly and time consuming measure. They create

considerable downtime. Further, the life of an aero-structure is largely based on the assumed load history rather than the particular load history of each individual aero-structure. A means of recording a load history would lead to a more precise estimation of inspection intervals and fatigue life [2].

As previously mentioned, structural health monitoring developments could lead to the development of smart structures which are able to employ corrective actions should an actuation and control system be implemented; however a reliable form of self-diagnosis is a necessary first step in this evolution. Various aspects of the structural health monitoring system must be proven satisfactory such as the installation, integration, system reliability, durability, replacement, reparability, data handling, integration and prognosis [3].

2 Composite Materials

2.1 Introduction

The use of composite materials is on the rise in the aerospace industry. Emerging large and medium sized aircrafts have increased usage of composite materials, largely due to high strength and weight saving benefits [4, 5]. Composite materials have also gained popularity in many industries over the past few years. A composite material can be designed such that the maximum strength of the material is in the direction of the expected maximum stress or stresses. Further, there are many types of fibers, matrix resins and lay-up configurations that can be used depending on the application.

Current use of fiber reinforced polymers, FRPs, in aerospace applications has increased due to the desire for strong light-weight materials; as indicated by a high strength to weight ratio. In these applications a thermoset epoxy resin is usually used as the matrix material and the continuous fibers are most commonly carbon however, glass (S-type), aramid and boron fibers have also found applications in recent aircraft designs. In some instances, foam cores and honeycomb structures are also used.

2.2 Manufacturing Methods

There exists a number of composite material manufacturing methods, such as autoclave molding, filament winding, resin transfer molding, prepreg layup, pultrusion and tube rolling [6,7]. Each method has its own advantages and disadvantages. Manufacturing methods are often chosen based on cost, accessibility, material quality and complexity. A primitive method, largely used at the experimental stage, is the wet hand lay up method.

2.2.1 Wet Hand Lay Up Procedure

This method of composite fabrication is very simple and basic. It is largely utilized at a very preliminary stage of composite material design and evaluation. For example, it may

be desired to evaluate the use of one particular type of resin material with another, all the while utilizing the same fiber type. The use of this method could then be desired as a way to minimize cost of preliminary investigation. This method does not require the pre-impregnation of fiber layers prior to specimen lay up. Rather, the impregnation of the fiber layers is done once the fiber layers are laid onto the lay up surface, i.e. in process [8]. Impregnation is done by pouring the desired resin under and over the fiber fabric and then using a hand roller to remove voids and evenly distribute the resin. The thickness of the composite can be controlled using spacers. A release film is also used between the composite and the spacers, plates or mold. Should a specific mold be employed, the make up of the material, such as the fiber volume fraction, can be controlled by measuring the amount of resin to be used. However, should a mold not be employed then there will be excess resin surrounding the specimen and the controlling factor of the composite material make up would be the use of thickness controlling spacers. This is the case for flat specimen fabrication; which is desired for the making of coupon type specimens. There then exists excess resin surrounding the composite that needs to be removed after the material has cured.

2.3 Residual Stress

Residual stresses in composite materials are inevitable. They result mainly due to the mismatch in thermal expansion coefficients of the constituents of the material. In order to manufacture a composite material, the temperature must increase so that the initially liquid resin will cure and become solid. The temperature at which this occurs varies and it is also common to increase the pressure by means of an autoclave. It is assumed that the material is stress free prior to reaching the glass transition temperature of the matrix (resin) [6]. The glass transition temperature (GTT) is the temperature at which the matrix material begins to solidify and become hard. Further, this is a property of the matrix material and is usually above 150°C for thermoset resins. Since the maximum cure temperature is greater than the GTT, the fibers will expand, or contract, depending on their coefficient of thermal expansion, CTE; which differs from the matrix CTE. After the material has been subjected to the high temperature for a set amount of time, the

material is then cooled. The cooling process can be as simple as subjecting the material to room temperature until it has cooled to room temperature or it may be a prescribed procedure such as a step down process.

As the material is cooled, the constituent matrix and fibers will contract or expand depending again on their own CTE. Glass fibers and boron fibers have positive CTEs and hence will contract during cooling. However, carbon and aramid (Kevlar) fibers have negative CTEs and will expand upon cooling. More specifically, these negative thermal expansion coefficients for carbon and aramid are in the longitudinal direction; in the transverse direction these coefficients are positive. Of interest to note is that the values of CTE for common thermoset epoxy resins, as listed in reference 6, are an order of magnitude larger than the CTE for the fibers mentioned.

From the discussion above, one can deduce that the primary mechanism causing internal residual stresses in FRP composite materials is the difference in CTEs of the constituent materials; namely the matrix and reinforcing fibers. Further, these residual stresses can vary within and between each lamina of the composite laminate. However, the difference in CTEs is not the only mechanism responsible for the formation of residual stress. There are also effects caused by the glass transition temperature, chemical shrinkage/cure shrinkage and tool-part interaction [9]. During the curing process, polymers can shrink in addition to the shrinkage caused by thermal effects; which can be as high as 7% for a typical epoxy resin [9]. Further, the interaction between the material and the tool or part upon which it is placed during the curing process can also have an effect on the residual stress. Other factors may include resin rich areas within the material and inconsistencies in the constituents. Voids within the material will also affect the residual stress. The minimization of voids can be achieved by use of an autoclave for the curing process.

With many factors affecting the residual stress of the composite material, it is important to note that some of these factors will contribute locally; such as voids and resin rich areas. These local factors can largely be controlled through quality control methods.

The effect of the mismatch in coefficients of thermal expansion, CTEs, can be found theoretically by applying classical laminate theory to the proposed lay-up. However, this method can be ambiguous when dealing with the effects of interaction between the constituents and it can also rely on experimental evaluation for accurate results. Further, it does not take the cure shrinkage into account. Therefore, experimental methods for measuring the residual stress in composite materials due to curing are required.

2.4 Mechanical Properties

To calculate the Young's modulus of a unidirectional fiber reinforced polymer, FRP, the rule of mixtures is used. The rule of mixtures is essentially a ratio formula, (1). The modulus is dependent on the moduli of the matrix material and the fibers, E_m and E_f respectively, and the percentage of each. This percentage is referred to as the fiber volume ratio, V_f , and is the percentage of which the FRP is composed of fiber. Similarly, the matrix volume ratio, V_m , is the percentage of matrix material within the material. Ideally, the sum of these two volume ratios would equal one however; this may not be the case due to the presents of voids within the material.

$$E_1 = V_f E_{1f} + V_m E_m \quad (1)$$

Further, it should be noted that the subscript 1 is used for the longitudinal direction of the continuous fiber by convention. This notation is important as some fiber types have a different modulus in the transverse direction, denoted by the subscript 2. The matrix material however is an isotropic material hence this notation is not required for the matrix.

If it is assumed that both the matrix and the fibers are under equal and uniform stress, the following relation for the transverse modulus applies.

$$E_2 = \frac{E_{2f} E_m}{V_f E_m + V_m E_{2f}} \quad (2)$$

Modifications to or variations of the above equation can also be used when determining the transverse modulus of a lamina [6]; however are not discussed here. Such is the case if a more accurate value for the transverse modulus is desired as the stress is simply not uniform for both the matrix and the fibers. If the material is in a non damaged state, continuity dictates that, when subjected to a load, the matrix and fibers are under equal strain. Since the moduli for the constituents are different, the stress can therefore not be equal. This can be illustrated using photoelasticity. Isochromatics are lines that join areas of equal maximum shear stress and can be seen in the photoelastic model image of Figure 2.

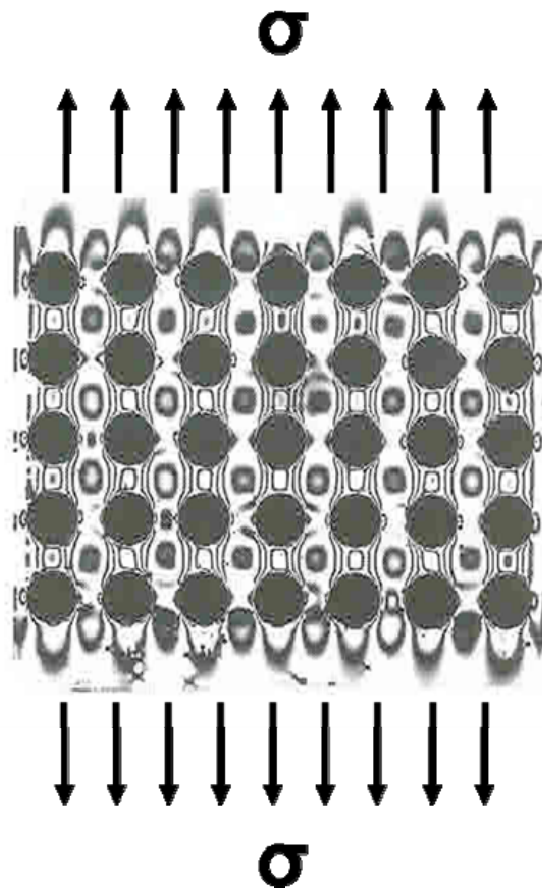


Figure 2 - Isochromatic Fringes of a Transversely Loaded Unidirectional Composite

Of main importance to note is that the very principle that makes continuous fiber composites have high stiffness in the longitudinal direction is what makes them weak in the transverse direction.

2.5 Fatigue Behavior

Fatigue damage is the cycle dependent degradation of internal integrity of a material. Fatigue behavior of composite materials is a complex phenomenon that consists of multiple damage/failure modes. The strength, stiffness, and remaining life of a FRP composite material will reduce as the number of loading cycles increase while it is accumulating fatigue damage. The micro events which reduce the strength, stiffness and determine the life of composite materials are complex, various and intricately related to a variety of failure modes in different circumstances. Hence, fatigue analysis can be quite a complex and involved issue.

Fatigue damage analysis of composite materials is quite different from that of fatigue damage of metal materials. This is due to the number of different damage mechanisms of composites that lead to the accumulation of damage; as oppose to damage propagation as seen in metals

It is believed that all fatigue damage processes are non-conservative [10]. This means that some of the energy that is introduced into the material by work being done on the material is not stored as strain energy. Rather, some of this energy is dissipated as a driving force for some internal processes. These processes include micro-crack formation or growth, thermodynamic events such as the rearrangement of molecular or atomic morphology (diffusion, grain boundary motion, etc.), chemical events such as stress-assisted corrosion, and a variety of other internal events [10].

Not all non-conservative processes produce fatigue damage in the sense that it reduces the remaining stiffness, strength or life, however it is believed that all fatigue damage processes are non-conservative. These non-conservative processes lead to irreversible

changes in the material that can result in layer delamination, matrix cracking, fiber splitting and fiber/matrix de-bonding. As these irreversible changes grow and/or accumulate the material stiffness, strength and remaining life are affected.

As there are a number of damage mechanisms and failure modes that the fatigue behavior depends upon, there are a number of contributing factors to this behavior. It is the polymer matrix that is of most interest as the fibers themselves are quite stiff in comparison and the fatiguing of the fibers alone is not normally considered. However, due to the viscoelastic nature of the polymer, stress concentrations in the vicinity of the matrix crack tip can influence the integrity of the stiff fibers [11].

There are other factors that affect fatigue behavior of polymers that are not normally seen in metals. Polymers have a greater dependence of cycling frequency due to internal heating and their low conductance. The cross linking of the polymer chains themselves is said to have an effect [11]. Polymers can exhibit large amounts of viscoelastic behaviors depending on time, temperature, polymer type and molecular structure. Viscoelastic creep can be a factor requiring consideration; especially at high temperatures, for extended periods of time and/or at high mean stresses or strains [12].

Currently there are no MIL spec standards for the design and analysis of composites for fatigue [13]. However, this section is reserved for future use which indicates that the importance of further understanding is recognized and this area of study is still maturing.

The study and analysis of FRP composite material fatigue is complex and involves many factors. There are theoretically based and experimentally based models for use in fatigue behavior predictions and analysis. For a more in-depth discussion, the reader is referred to reference [14].

3 Fiber Optic Sensors

3.1 Introduction

The use and development of fiber optic sensors has increased in recent years. They are an attractive means for structural health applications due to their small size, usually less than 250 μm , light weight, electromagnetic neutrality and the ability to include a number of sensors on a single fiber optic.

The anatomy of a fiber optic includes an inner core, cladding and external buffer. The buffer is a protective layer. The core and cladding of the fiber optic is usually composed of silica glass or quartz. Light is channeled through the core of the fiber utilizing the principle of total internal reflection due to the different indexes of refraction of the core and cladding [15].

3.2 Principle of Operation

Fiber optics guide light from a source to a destination. This is done by utilizing the principle of total internal reflection as described by Snell's law, or the law of refraction. Snell's law is shown in equation (3). When light passes from one medium to another, where each medium has a different index of refraction, n , the light will refract accordingly, depending on the angle at which the light enters the medium, known as the angle of incidence, θ , as measured from the outward normal, shown in Figure 3.

$$n_1 \sin\theta_1 = n_2 \sin\theta_2 \quad (3)$$

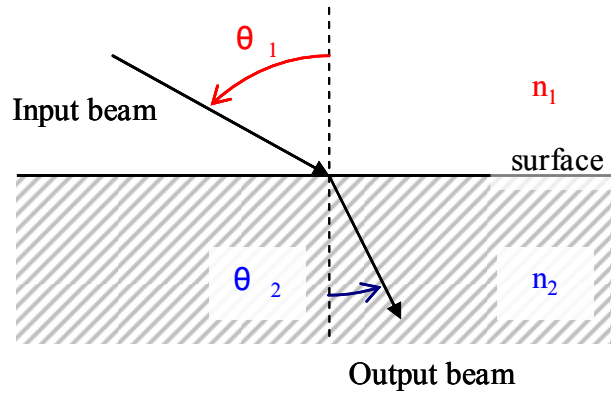


Figure 3 - Law of Refraction

There is a critical angle at which the light will not pass into the second medium, rather it will reflect. This angle is known as the critical angle and is described by equation (4), which can be derived from Snell's law by setting θ_2 to ninety degrees and isolating for θ_1 .

$$\theta_c = \sin^{-1} \frac{n_2}{n_1} \quad (4)$$

The application of this principle in the use of fiber optics is illustrated in Figure 4. One type of glass is coated with another type of glass with a different index of refraction. The glass in the center is known as the core and the glass which coats it is known as the cladding. It should be noted that the index of refraction of the core, n_1 , is greater than the index of refraction of the cladding, n_2 . Light with an angle of incidence larger than the critical angle will travel through the core and light with a smaller angle of incidence will pass into the cladding. It is the light that travels through the core that is of interest.

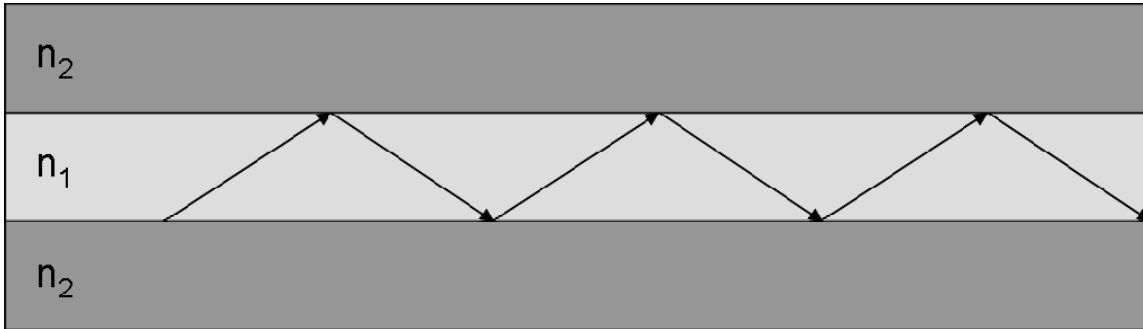


Figure 4 - Core and Cladding

The anatomy of a fiber optic can be seen in Figure 5. The buffer is commonly a polyacrylate coating that protects the cladding and core of the fiber, however can be a different material. The bare fiber, cladding and core, is quite fragile as it is very thin, therefore it needs to be protected by the buffer and occasionally also a jacket.

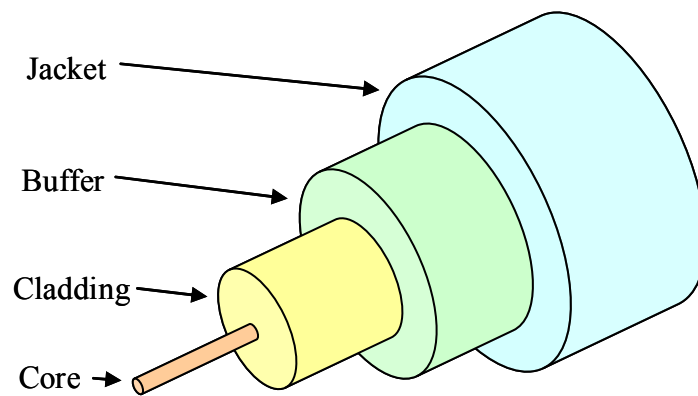


Figure 5 - Anatomy of a Fiber Optic

It may also be desired to further protect the fiber due to abrasive conditions. In this case an external jacket can be applied to the fiber, making the fiber optic more resistant to damage.

When a sensor, or grating, is written on the fiber optic, the jacket and buffer need to be stripped off, exposing the bare fiber. The bare fiber, cladding and core, can then be recoated with the buffer material or with a polyimide coating. Polyimide coating not

only helps to protect the bare fiber, but also assists with adhesion when the sensor, or grating, is bonded to a material, or embedded into a material. This is an important part of the overall process since debonding of the sensor at ‘high’ strain levels will not give accurate strain measurements

A number of sensors can be written onto a single fiber; often called an array or fiber optic array. These fibers can then be multiplexed by means of a coupler as shown in Figure 6.

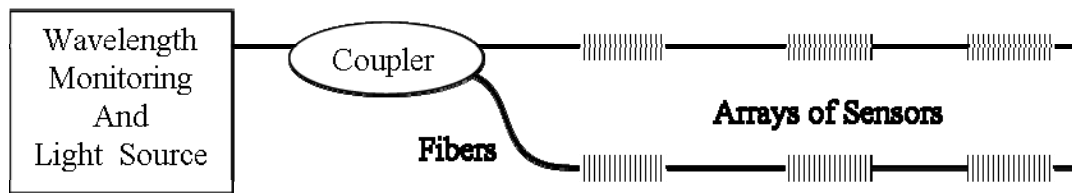


Figure 6 - Fiber Optic Multiplexing

This set up can result in a network of parallel fiber optic arrays all monitored by the same system.

Fiber optics have high strength in the longitudinal direction of the fiber; however can be easily sheared due to their thinness. Thusly, they can be damaged or broken if not adequately handled and/or protected.

3.3 Fiber Bragg Grating

A Fiber Bragg Grating (FBG) is a periodic perturbation of the refractive index along the fiber length which is formed by exposure of the core to an intense optical interference pattern [16]. A common method used to write the grating is known as phase masking or the phase masking technique. This method is preferred since the ultraviolet light used can be aimed at the side of the fiber to write the grating. As previously mentioned, the jacket and/or buffer need to be removed from the fiber prior to the writing process.

The perturbations of the refractive index are illustrated in Figure 7. In this figure, the periodic change of the refractive index is illustrated by different shades of white and black. It is only the core of the fiber that has these perturbations. The distance between the peak indexes is known as the pitch, Λ .

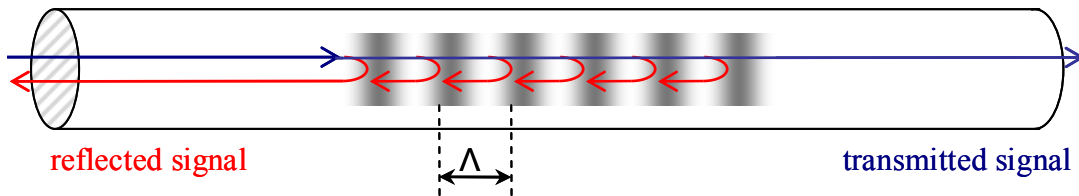


Figure 7 – Perturbations of the Refractive Index

Should there be no grating written, all the light in the core of the fiber will continue along the fiber. At the grating, light centered of a particular wavelength will be reflected back in the direction that it came from. This particular wavelength, λ , is governed by the index of refraction of the grating (or effective index) and the pitch. This wavelength can be found via equation (5) below. The wavelength λ is also referred to as the Bragg wavelength or λ_B .

$$\lambda = 2n\Lambda \quad (5)$$

The light that travels through the fiber originates from a broadband light source. Hence, the light has multiple wavelengths; which is dependent on the source used. When the light reaches the grating, only the wavelength corresponding to the one dictated by equation (5) is reflected back towards the source. All other wavelengths are transmitted through the fiber. Since the reflected wavelength is dependent upon the grating pitch, an applied strain will result in a change of grating pitch and hence a wavelength change, or shift, of the reflected signal. This sensing concept is illustrated in Figure 8.

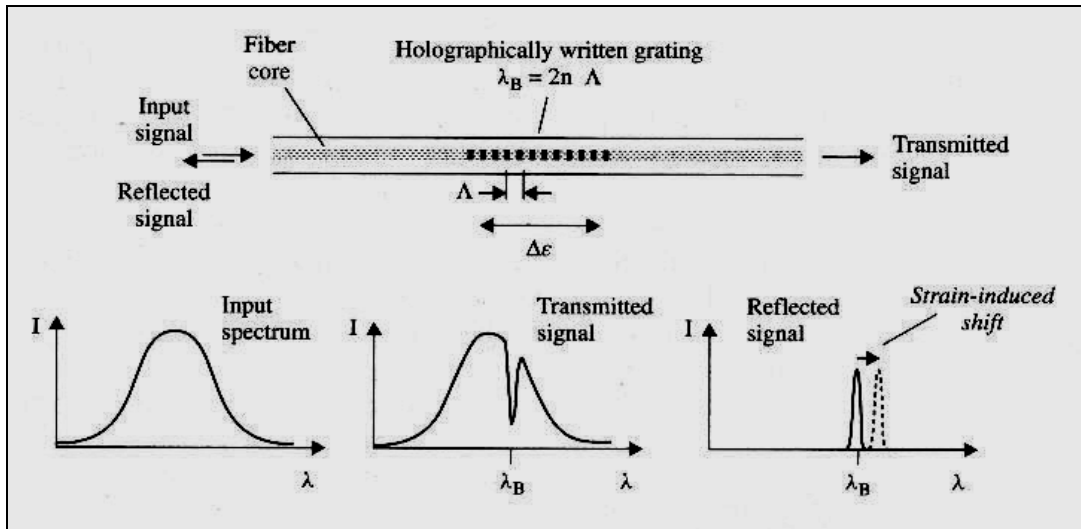


Figure 8 - Sensing Concept of FBGs [19]

The fiber needs to be connected to two vital pieces of equipment; a broadband light source and a means of wavelength monitoring. These two pieces of equipment can be attached to a coupler which is in turn attached to the fiber optic, as shown in Figure 9. Some modern equipment has these two pieces built into one; such as an interrogator.

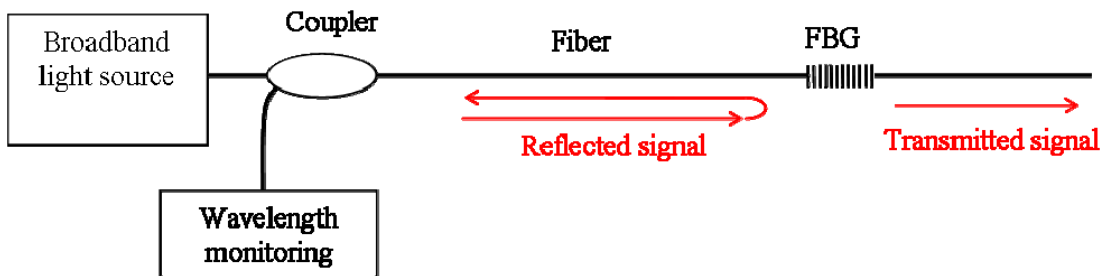


Figure 9 - Standard Setup

The intensity of the wavelengths of light is usually measured in decibels, dB. The decibel is a logarithm of a ratio; in this case of power, P.

$$P_{dB} = 10 \log_{10} \frac{P_1}{P_0} \quad (6)$$

It is also common to express the light intensity linearly. P_0 can be a reference value; for optics 1 nW is used.

$$P_1 = 10^{\frac{P_{dB}}{10}} P_0 \quad (7)$$

In the literature on fiber optic strain sensors both methods of wavelength intensity measurements are observed.

In order to assess the strain sensed by the FBG, a reference wavelength must be known. The reference wavelength can be the unstressed state or a stressed state, depending on the application of use. The corresponding wavelength shift between the reference wavelength and the strain induced wavelength yields the corresponding strain once the proper factor is applied. The exact factor is dependent on the fiber optic used, however, is usually in the range of 1 pico-meter per micro-strain. Further, proper calibration of the sensing equipment can be done to the nearest pico-meter and hence the nearest micro-strain.

Recalling equation (5), the index of refraction of the core is elemental to the reflected wavelength. However, this value is an effective value that is often referred to as the effective index of refraction, n_{eff} . The reason for this is illustrated in Figure 10. The actually index of refraction varies periodically along the grating.

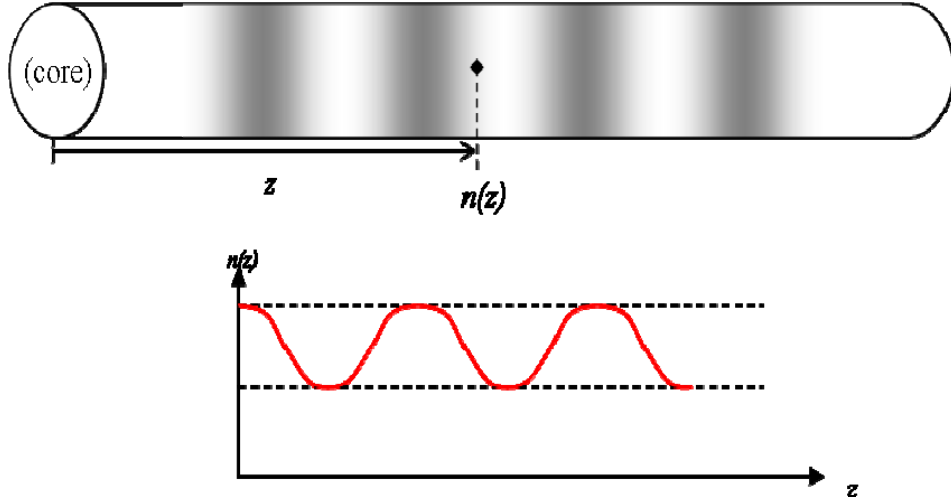


Figure 10 - Periodic Change in Index of Refraction

The equation for the change in wavelength with a change in strain can be found by differentiating equation (5) with respect to strain. The result is shown in equation (8).

$$\frac{d\lambda}{d\varepsilon} = 2 \left(n_e \frac{d\Lambda}{d\varepsilon} + \Lambda \frac{dn_e}{d\varepsilon} \right) \quad (8)$$

As the above equation dictates, a change, or shift, of a peak wavelength, or Bragg wavelength is a function of the rate of change of pitch with strain and the rate of change of the effective refractive index with strain.

The reflected wavelength not only changes with strain but with temperature as well. Differentiating equation (5) with respect to temperature yields equation (9).

$$\frac{d\lambda}{dT} = 2 \left(n_e \frac{d\Lambda}{dT} + \Lambda \frac{dn_e}{dT} \right) \quad (9)$$

The above equation is analogous to equation (8) except it is with respect to temperature and not strain. In this instance it is the last term in the parentheses that is of dominance.

The change in effective index of refraction is more sensitive to a change in temperature than changes in strain. Further, a change in strain has a greater effect on the change of pitch of a grating. The change in pitch of a grating due to temperature is dependent of a fibers coefficient of thermal expansion; which is usually quite small and depends on the fiber type.

Of importance to note is that the two effects on the reflected wavelength of a grating are not separable. That is to say that one cannot measure a change in strain and a change in temperature simultaneously. Therefore, a means of compensation must be applied if one of these variables is not held constant.

3.4 Other Types of Fiber Optic Sensors

There exists a variety of fiber optic sensors. Only sensors within the fiber Bragg grating family are mentioned here for clarity.

The use of chirped grating is on the rise due to their apparent ability to measure strain distributions. A chirped grating is written in the same manner as regular fiber Bragg gratings except that the phase mask used is specific for these types of gratings in that they do not have a uniform pitch, Λ . This is illustrated in Figure 11. The resulting peaks are broad in nature.

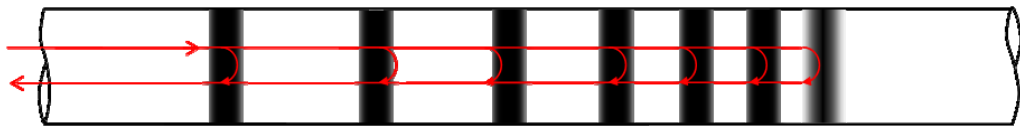


Figure 11 - Chirped Grating

The cross section of another type of fiber optic sensor is shown in Figure 12. These are high birefringent fibers capable of two dimensional strain measurements.

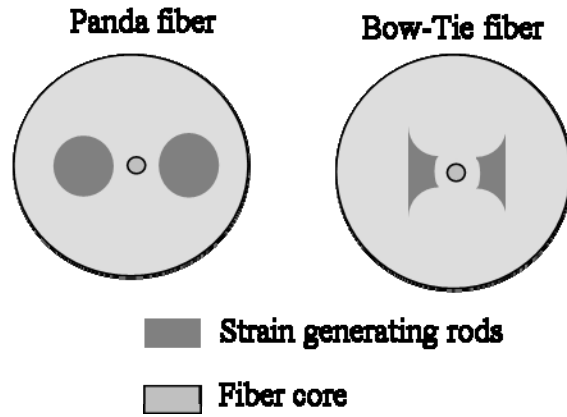


Figure 12 – Panda and Bow-tie fibers

An inherent difficulty with these types of fibers is ensuring proper orientation of the lateral axis.

4 Internal Monitoring of FRPs with Embedded Fiber Optic Sensors

The uses and applications of embedded fiber optic sensors in composite materials are evolving. This is an attractive application as an embedded fiber optic sensor can relate internal material health information of a composite part that may not be detectable visually; this may include delamination and internal matrix cracking. A couple of recent developments in the uses of embedded fiber optic sensors include distributed strain sensing [17] and detection of environmental acid penetration [20].

Care must be exercised to ensure that the fiber optic is not damaged where it exits the composite. For this reason, protective materials are used to surround the fiber at the exit. Such examples include affixing a plastic plug around the fiber exit [21] and surrounding the fiber with a steel tube as well as a polymer jacket [22].

Of relevance to the aerospace community is experimentation of embedded fiber optic sensors in a carbon FRP aircraft skin panel [23]. The researchers state that the resulting system is quite robust and it seems that the embedded sensors could stand the hostile operational life environment of aeronautic structures.

4.1 Material Fabrication

As previously discussed, material fabrication methods vary and can be simple or complex. There is a desire to monitor the process internally to ensure the quality of material desired. Resin rich areas, dry spots and voids can degrade the strength of the material. Embedded fiber optic sensors have gained much attention for this application. There have been successful applications of embedded FBGs providing information on the fabrication process and the residual stress of the material.

Real time monitoring to the reflected spectrum during vacuum-assisted resin transfer molding can provide information on the resin flow via temperature difference and observed shrinkage [24]. During RTM fabrication, embedded FBG sensors can detect timing when viscosity and stiffness of the resin become high enough to constrain the sensor [25]. Other examples of the use of FBG sensor for cure monitoring can be found in references [26, 27 & 28]. It should be noted that due to the inability to separate wavelength shifts due to temperature and strain, a means of temperature compensation is required. This is often achieved by using a reference FBG if possible. A reference grating would provide the temperature induced shift that can then be subtracted from the total shift in the embedded grating, yielding the mechanical strain induced shift. Further, this use of a reference grating can be employed for the same purpose through out the curing process in order to monitor the formation of residual strain.

Theoretical evaluation of residual stress can be very complex. Methods and models have been proposed, some more accurate than others. The authors of reference [29] used the viscoelastic model to calculate the residual stresses of specimens that they also fabricated with an embedded FBG to measure the residual stress. It was their finding that the two where in close agreement. This particular model was chosen based on its high accuracy.

4.2 Specimen Testing

Expanding the application parameters and uses for embedded fiber optic sensors is still a matter of current research. There are some parameters that have been established and accepted by current researchers. One such parameter is related to the placement of the fiber optic. It has been shown that the placement of the fiber optic in the direction of the continuous fiber bundles has no degrading effect on the surrounding host material [30 & 31]. This is also true if the fiber is placed in the direction of the continuous fibers at an interface of a transverse ply. The presents of the fiber optic can aid in resistance to matrix crack growth [32].

It cannot be assumed that embedding a fiber optic sensor into a FRP has no effect on the sensor. It is reported that an embedded FBG loses intensity after it has been embedded and the peaks broaden [25 & 33].

The sensing principles previously discussed for a FBG have been simplified for one dimension. More complex theory includes the strain optic coefficients of the fiber itself, in three dimensions. This becomes of interest when strains become large and the transverse strains can no longer be neglected. Transverse strain causes the reflectance spectrum to split into two peaks and the bandwidth between these peaks contain information on the transverse strain [33]. The authors of reference [34] attribute the splitting of the peaks to the strain induced birefringence effects in the core of the fiber. However, it has also been suggested that this birefringence effects may not be substantial as they are not witnessed by all researchers [24, 35]. This phenomenon of peak splitting can be partly dependent on the type of coating surrounding the sensor. Peak splitting occurs for sensors not coated with any type of coating, for temperature induced shifts, where as the peaks did not split for sensors coated with polyimide [36]. Further, most current researchers utilize the benefits of polyimide coated FBGs as it also improve adhesion characteristics.

Small diameter fibers are often used for embedding FBGs in FRPs. Since they can be half the size of the normal fiber, they are attractive in the sense that they may be less intrusive than regular fibers. However, one main drawback with this fiber type is that the reflected peaks are quite broad in nature. This broadening is further enhanced when the sensor is strained [36]. These types of sensors however are stated to be under development by the author of reference [37] and have been shown by the same researcher to be capable of detecting and monitoring the transverse crack evolution in composite laminates.

4.2.1 Fatigue Testing

In a preliminary study, [38], to investigate the ability of an FBG to detect a stiffness drop in a fatigued FRP specimen a FBG was mounted to the surface of the specimen and compared with the readings of an extensometer. The surface mounted FBG showed good correlation with the extensometer during the duration of the test, in which case a stiffness drop did occur and was detected by both means of measurement. However, during the course of the testing a severe broadening of the peak was observed. It was suggested that this was due to the debonding of the sensor from the surface of the specimen and that perhaps this issue may be resolved by embedding the sensor.

Intensity based fiber optic sensors were embedded into a specimen and fatigue tested [22]. This type of sensor differs from an FBG. The main principle is that a gap in the fiber, surrounded by a capillary tube held on by beads of epoxy, will lose light intensity as the gap is strained. Regardless, the sensor showed good comparison with an extensometer throughout the duration of testing; both of which detected a drop in stiffness of the specimen. The sensor ultimately failed at the ends of the capillary tube.

A specimen with an embedded FBG and a surface mounted extensometer was cycled and data was collected during the cycles [25]. The strain values during cycling agreed well with the extensometer readings. In this study, the specimen was not damaged and the fiber optic remained intact. No comments were made on damage detection as the specimen remained undamaged throughout the 100,000 cycle test.

Fatigue testing of a couple of specimens with embedded FBGs and a hole drilled in the specimen did not yield any conclusive evidence of a FBGs ability to detect fatigue damage [39]. It is interesting to note that the authors are referring to the ability to detect fatigue damage based on a change in the light intensity and peak wavelength with cycles. However, the authors did note that a shift in the wavelength reflects a change in the internal strain around the FBG. Further, they did state that a broadening of the peak and a sharp drop in light intensity seem to be associated with the onset of matrix cracking and localized delamination. These same authors expand their research efforts and compare

FBG readings of damaged specimens with C-scan and X-ray [40]. They qualitatively show that FBGs have the potential to detect fatigue damage. Similar results were found with a FBG embedded in a braided composite [41]. It was stated that observation of the reflected spectrum has the ability to indicate internal damage.

5 Specimen Fabrication

The goal was to fabricate coupon type specimens with a fiber optic sensor embedded in between the central layers of knitted fabrics using a wet hand lay up method. Two preliminary specimens were fabricated to further define the issues involved in extracting a fiber optic from the specimen as well as to experiment with possible fiber protection/extraction methods. In each case a flexible protective tube was set in place around the fiber optic at the exit. The protective tube is approximately one millimeter in diameter. Further, a flexible tube was desired in order to fit the specimen into the appropriate testing equipment after fabrication.

Although only one end of the fiber optic is required to exit the specimen in order to obtain a reading from the sensors, it was decided to have both ends of the fiber exit the specimen undamaged. This is due to the fact that the possibility does exist that one end of the fiber may become damaged during handling and testing. Should this occur, the other end of the fiber optic could then be used and thereby not hinder the specimen unusable for testing.

The resin used in this study was an epoxy resin for each specimen. A variety of unidirectional fiber bundle knitted fabrics were used. Fiber Bragg grating sensors were the fiber optic sensors considered during the process.

5.1 Preliminary Specimens

5.1.1 Fiber Placement Experimentation

At first it was desired to have the fiber optic exit the side of the specimen so that the mechanical grips of the test frame would not interfere with the fiber optics function. This was a challenge since the sensors needed to be placed in the longitudinal direction of the

specimen rather than the transverse as this was the direction that was desired for future measurements. The first fiber optic array layout is shown in Figure 13.

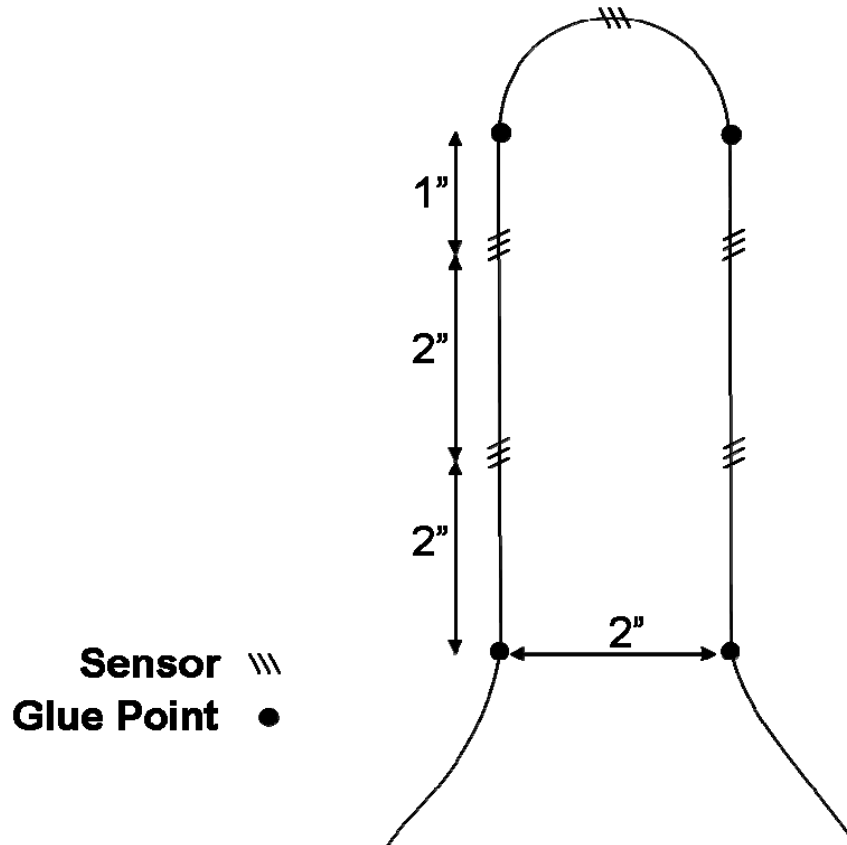


Figure 13 - First Fiber Optic Array Layout

Two main difficulties arose during the fabrication of trial specimens with this layout. The first issue was the concern that the glue used to hold the fiber in place would impregnate the fiber bundles of the fabric and therefore affect the mechanical properties of the composite material in the vicinity of the glue point. The glue points were necessary in this layout design as the resin alone was not viscous enough to hold the fiber in place during the fabrication. Further, as the temperature of the resin increased during the curing cycle, the viscosity would decrease thereby lessening the likelihood that the resin could hold the fiber in place during the entire process.

Three trial specimens were created with three different types of glue; 100% cyanoacrylate, a rapid cure epoxy and a standard epoxy. The specimens were coupon like in size and

were fabricated using glass fiber fabrics. The fiber optic was glued to the bottom layer of fabric during fabrication.

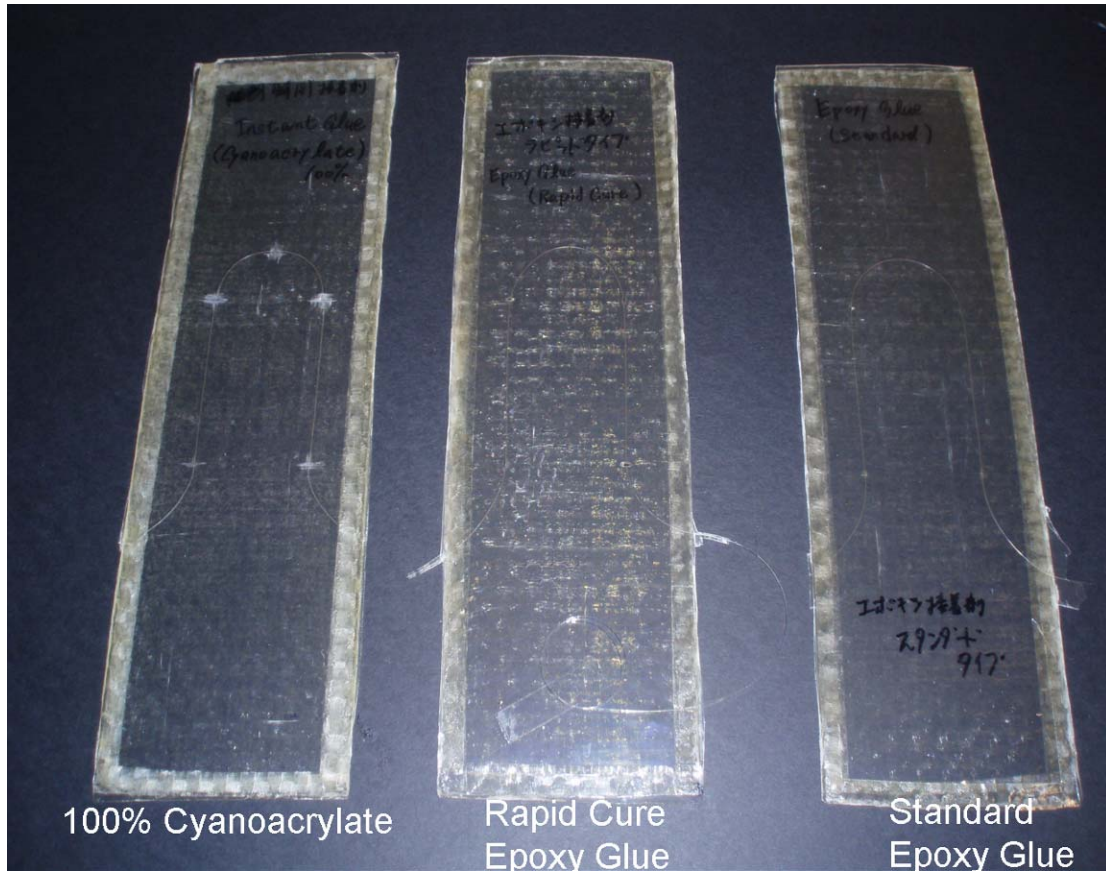


Figure 14 - Glue Trial Specimens

After curing, it was possible to see the result of the glue points. Upon visual inspection, the cyanoacrylate was seen to be the most obtrusive on the surrounding material. The rapid cure epoxy was the second most obtrusive. The standard epoxy glue was found to be the most benign. This is further reflected by the figure below.

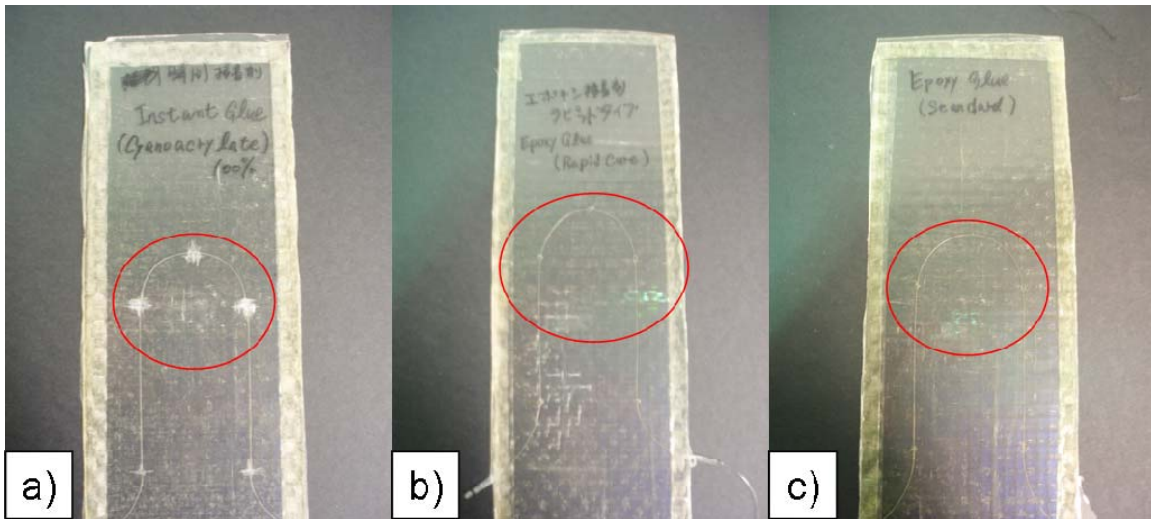


Figure 15 - Glue Trial Specimens a) Cyanoacrylate b) Rapid Cure Epoxy and c) Standard Epoxy

A main drawback of standard epoxy is the long cure time. The fiber needs to be held in place during this time.

5.1.2 First Specimen

The first specimen was fabricated without making any alterations to the process to account for the fiber optic. The fiber optic and protective tubing was set in place after the bottom layer of fabric was impregnated with the resin material. The top layer of fabric was then set into place and impregnated. Prior to preparing the specimen for curing, the fiber optic and protective tubing were adjusted so that the fiber optic was located at the widthwise center of the specimen. The protective tubing was embedded one centimeter into the specimen.

After the cure cycle was complete, the release film was removed. An attempt was then made to remove the excess resin, both by hand and by cutting. This resulted in damage to the fiber optic.

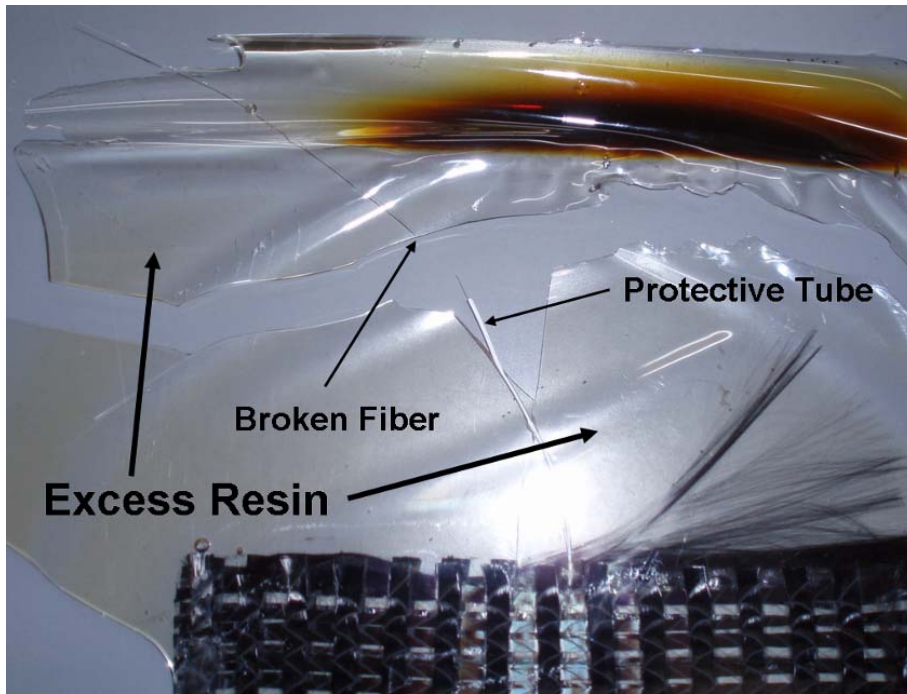


Figure 16 - First Specimen with Damaged Fiber Optic

This is illustrative of the difficulty of extracting a fiber optic from excess resin surrounding a composite specimen fabricated using this process. Further, the difficulty becomes larger as the thickness of the specimen increases, thusly resulting in the excess resin being thicker as well.

5.1.3 Second Specimen

Based on the findings from the first preliminary specimen, a second specimen was constructed. Two methods were used; the clay method and the reduced resin method. The clay method consists of coating the fiber optic and protective tubing at the exit with a high cure temperature clay that would not cure at the curing temperature of the resin. The reduced resin method consists of attempting to reduce the amount of resin at the fiber optic exit in order to make extraction of the fiber by previous methods more feasible.

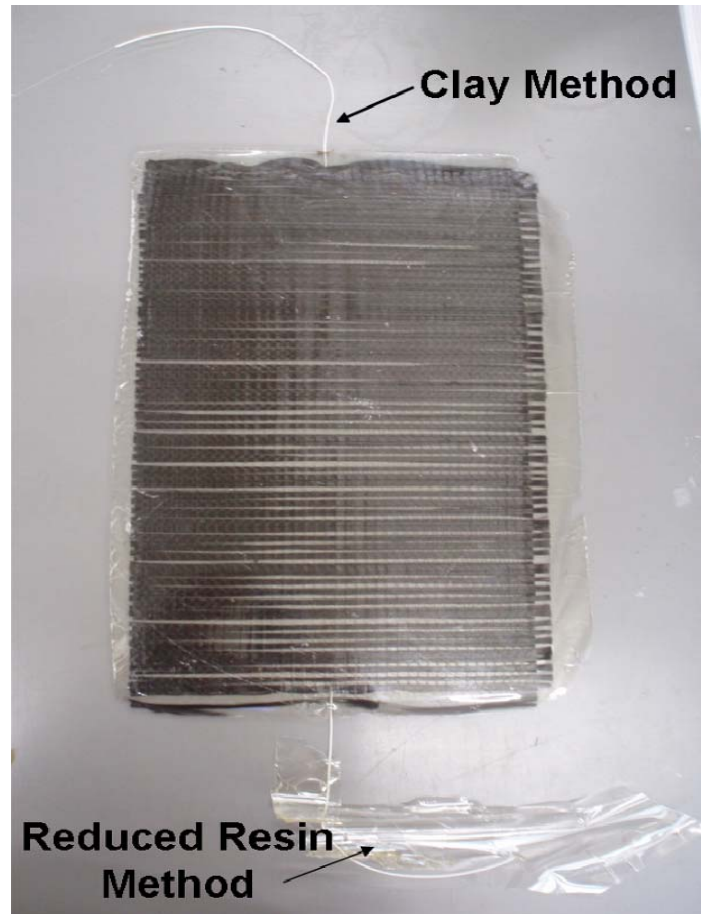


Figure 17 - Specimen Constructed using Reduced Resin Method and Clay Method

The reduced resin method was not deemed successful as removal of the excess resin was still a difficult task. A crack had propagated in the resin and continued through the protective tubing and fiber optic, shearing the fiber optic, illustrated in Figure 18. Although this event may not occur in every instance, it is still indicative of the unreliability of this method especially when constructing larger specimens.

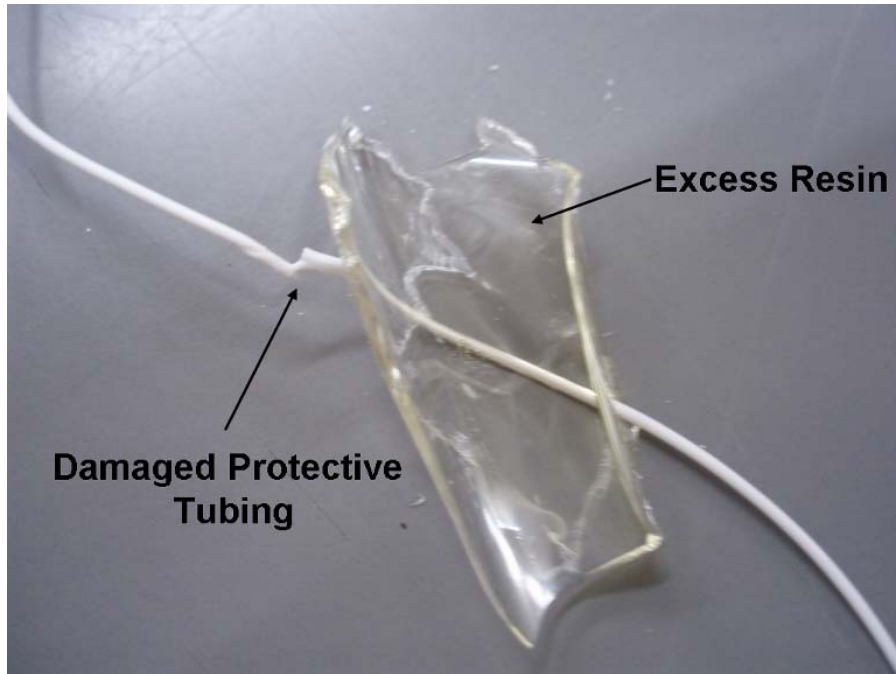


Figure 18 - Fiber Optic Damaged with Reduced Resin Method

The clay method on the other hand proved to be a more reliable means of fiber extraction. The protective tubing as well as the exposed fiber optic remained intact throughout the entire process. A minimal amount of residual clay was left on the specimen itself where the clay came into contact with the specimen. However, this is considered to be a non-intrusive byproduct of this method.

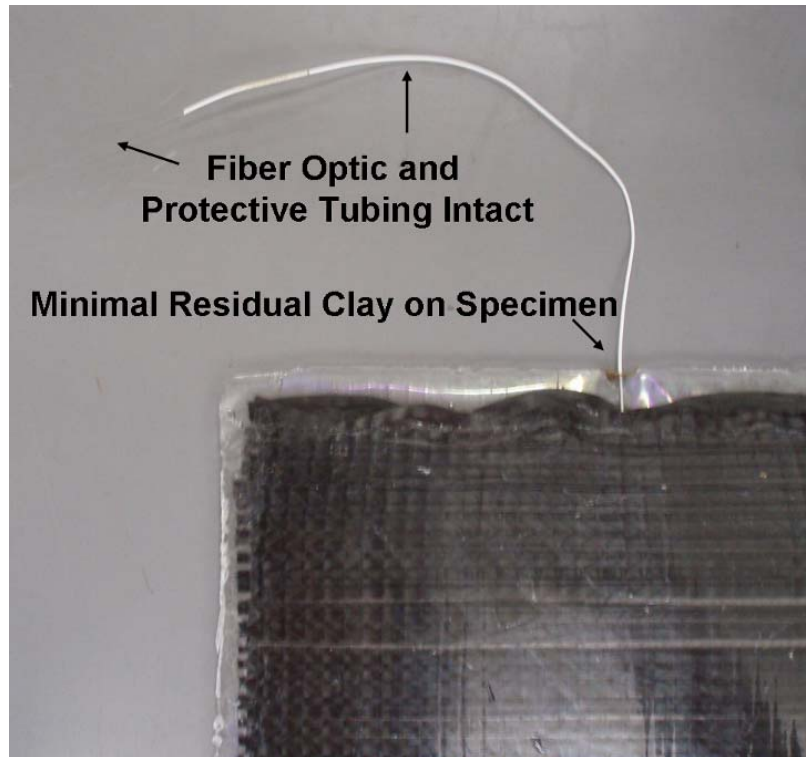


Figure 19 - Fiber Optic Intact with Clay Method

Based on the findings of this specimen, the clay method was selected to be further developed and is herein discussed in more detail.

5.2 Clay Method Procedure

5.2.1 Pre-cure

Once the protective tubing was put in place on the fiber optic, it was permanently affixed to the fabric. The method of affixation used in this instance was a standard cyanoacrylate adhesive due to ease of use and availability. The purpose of this step was to inhibit the fiber optic from moving during fabrication. Only the protective tubing was affixed to the fabric, not the fiber optic, so that affixation would not influence future readings from the sensors. However, this was a prerequisite in this instance and may not be of concern for further application of this process. The protective tubing was held in place by a piece of

clear tape while the adhesive dried. Approximately a quarter to a half of an inch of protective tubing was adhered to the fabric.

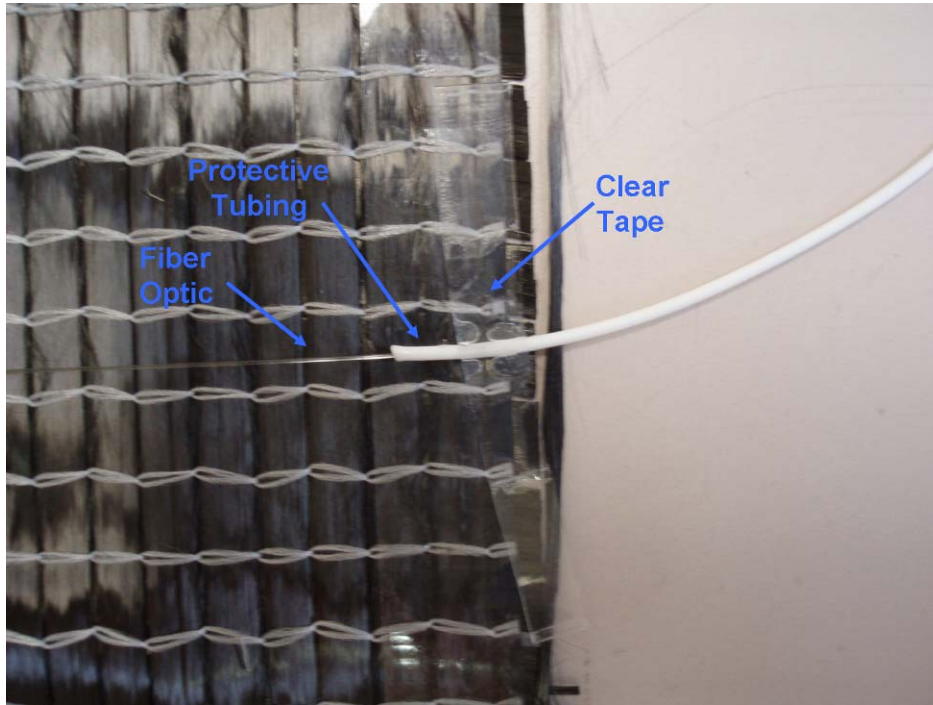


Figure 20 - Protective Tubing Affixed to Fabric

Four fiber optic arrays were set in place on each fabric. The size of the fabric was limited by the size of the oven available. Further, it was desired to fabricate a number of specimens at the same time to increase the uniformity of the specimens.

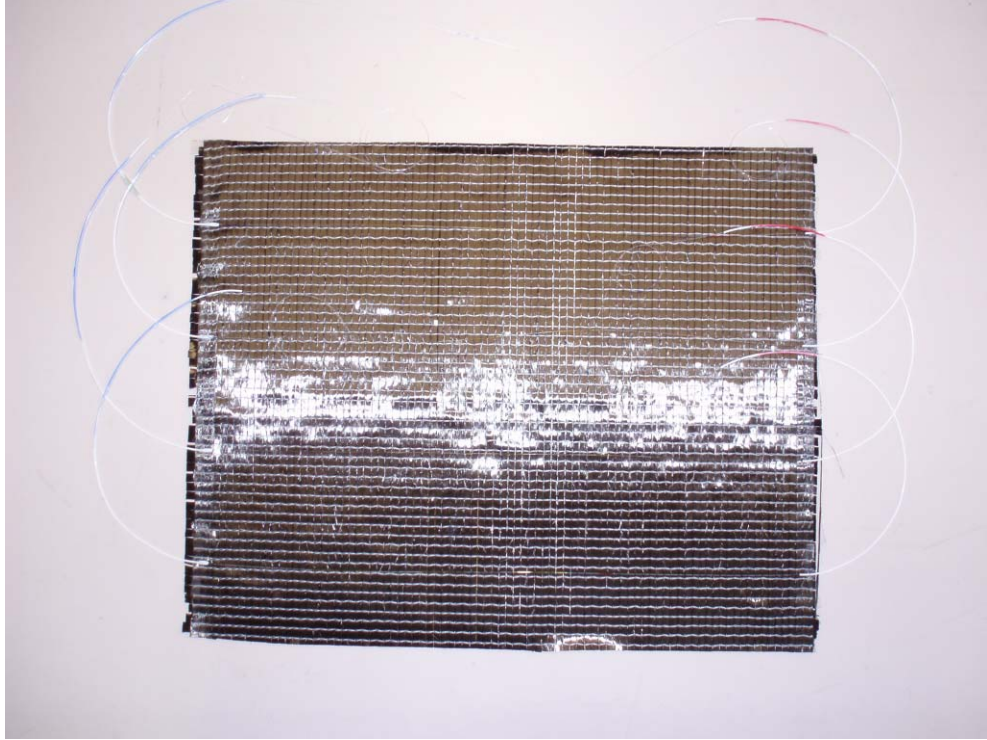


Figure 21 - Fabric with Fiber Optics in Place

Once the fiber optic sensors were in place, the fiber optic itself was marked where it exits the protective tubing away from the specimen. The tubing was then coated with the high cure temperature clay, by hand, giving the fiber optic, protective tubing and clay a diameter of approximately half an inch. Depending on the application, this diameter may need to be increased.



Figure 22 - Bottom Fabric Layer with Fiber Optics in Place

Impregnation of the first layer of fabric is then a delicate process. Extra care must be taken to ensure that the fiber optic is not damaged by the roller. It is necessary to have the protective tubing affixed to the fabric prior to this step of the process. This prevents movement of the fiber optic and clay, specifically the exit location, while the fabric is further impregnated and rolled.

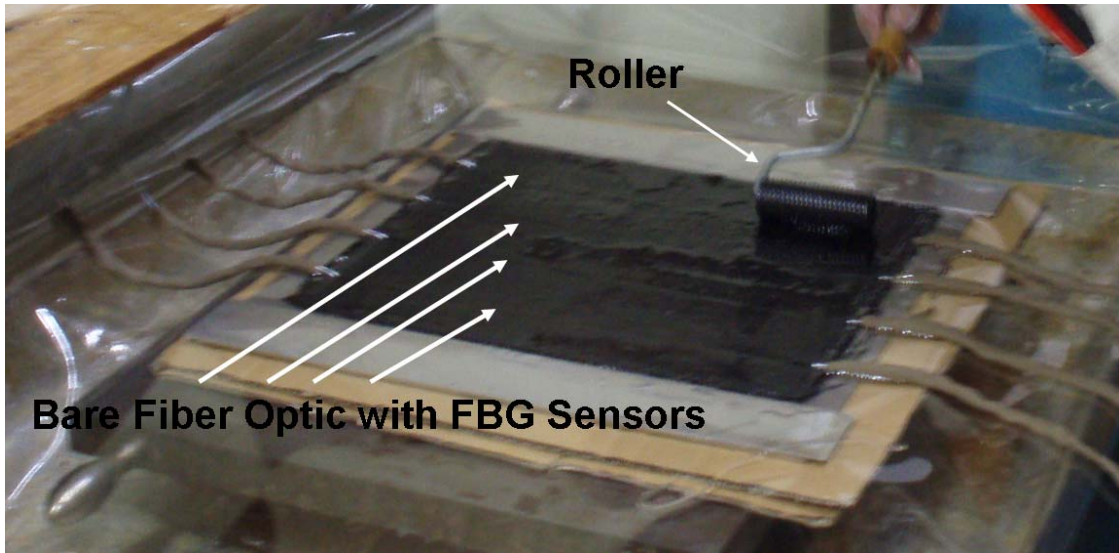


Figure 23 - Impregnation of Bottom Fabric Layers with Exposed Fiber Optics

Once the entire specimen has been impregnated and hand rolled it is necessary to ensure that the sensors are in the desired location as they may have moved during the hand rolling process. This is done by referencing the markings placed on the fiber optic itself as it exits the protective tubing. Thusly, having the fiber exit both sides of the specimen can be of benefit for this purpose. However, should it be deemed appropriate, affixing the fiber optic directly to the fabric may negate this step.

After the release film and appropriate spacers are in place, the remainder of the excess resin is then channeled out of the specimen. Figure 24 illustrates this and further shows how the clay is protecting the fiber optic from the excess resin.

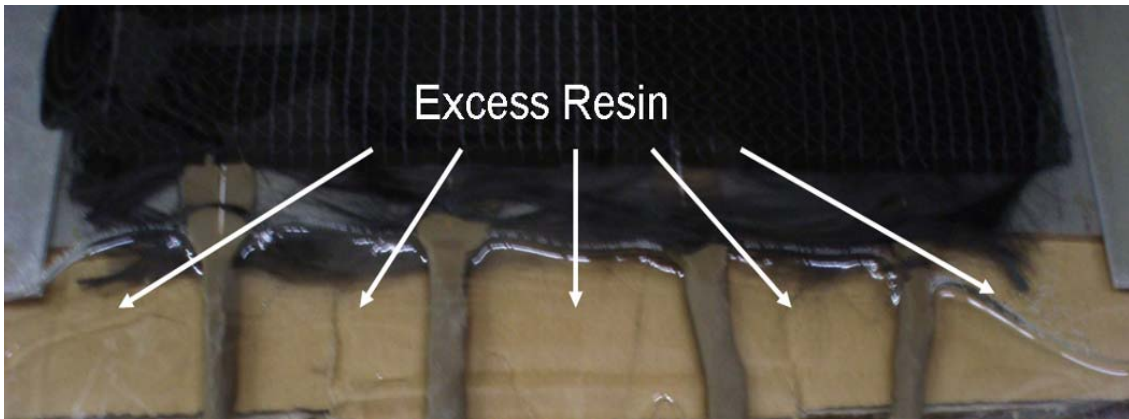


Figure 24 - Excess Resin and Fiber Exit Pre-cure

The specimen is now prepared for the cure cycle.

5.2.2 Post-cure

After specimen curing, the high cure temperature clay is slightly brittle in nature and can be removed quite easily by hand. The excess resin surrounding the fiber optic exit is fully cured.

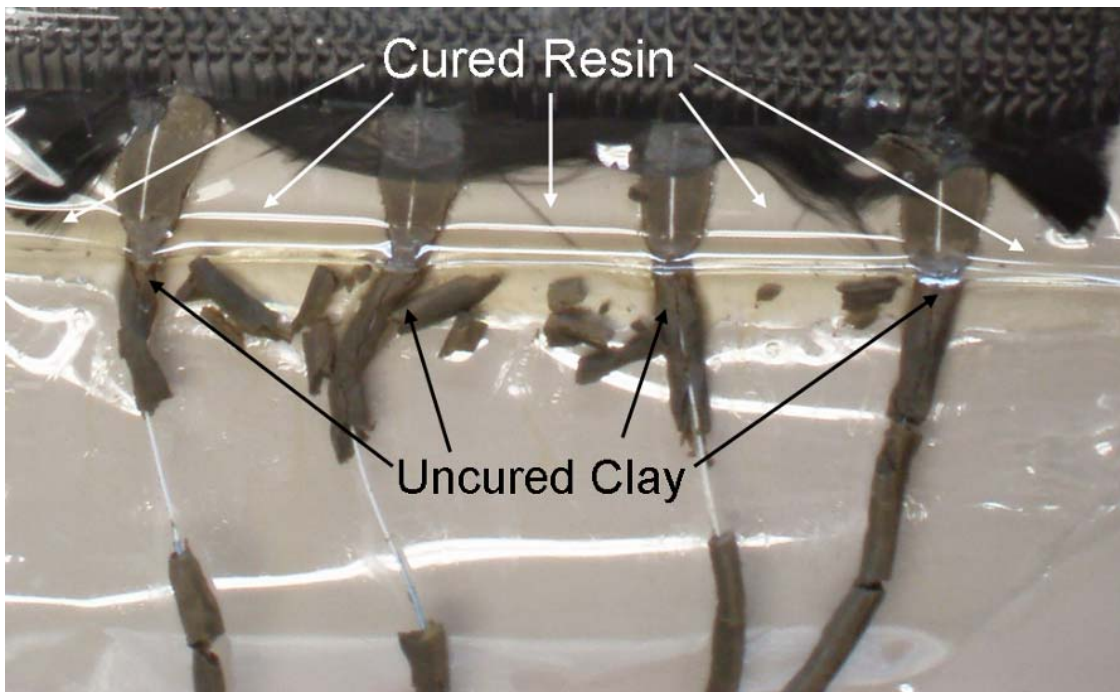


Figure 25 - Brittle Clay Post-cure

With all the clay removed, the protective tubing and fiber optic is exposed and free of damage.

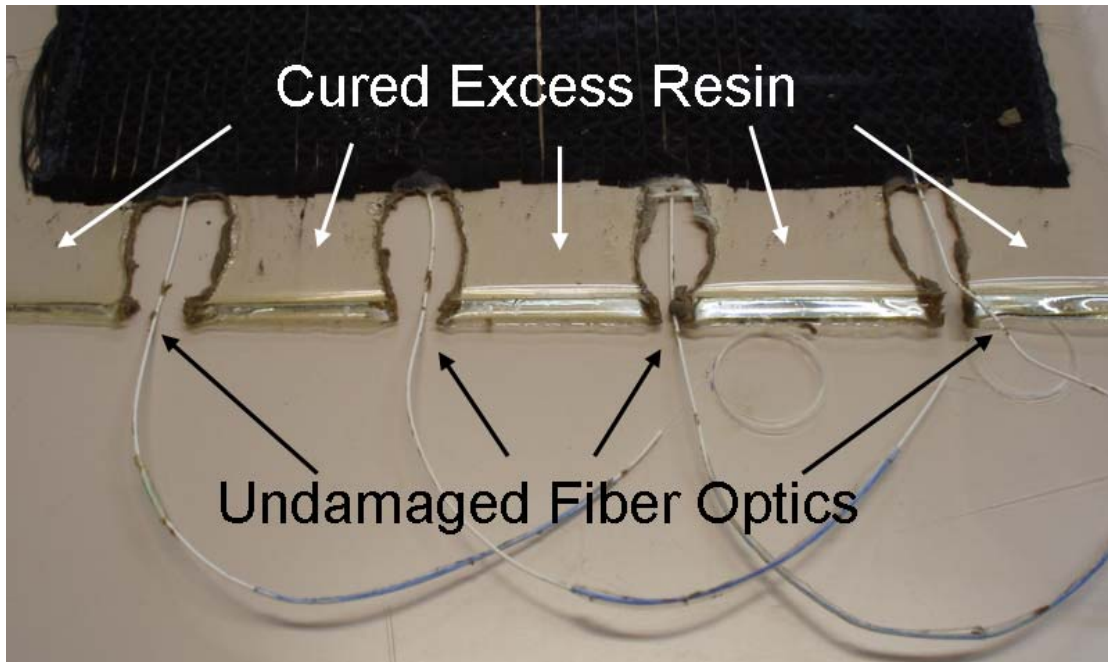


Figure 26 - Undamaged Fiber Optics Post-cure

Since the protective tubing is flexible, the tubing and fiber optics can be temporarily pulled back over the specimen to expose the excess resin. The excess resin surrounding the specimen can be removed by an appropriate cutting method; in this case a diamond disk saw was used.

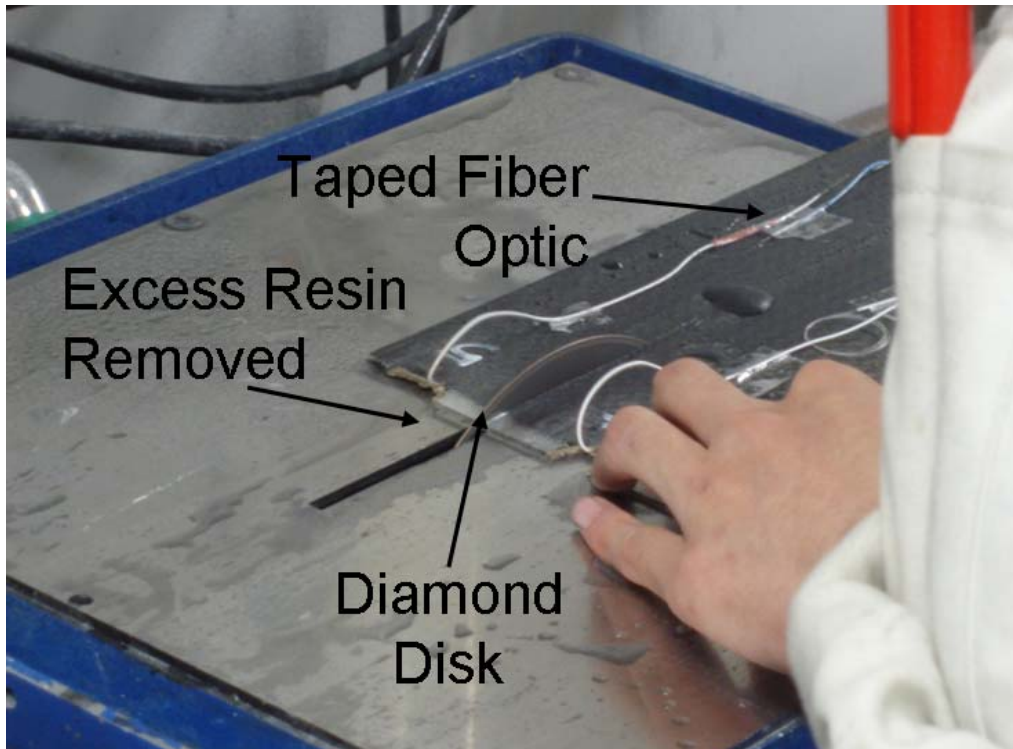


Figure 27 - Removal of Excess Resin and Specimen Cutting Post-cure

The degree of accuracy that the excess resin can be removed depends largely on the cutting method used. Care must be taken to ensure that the fiber optic is not cut during this process. Should a high level of accuracy be required it is recommended that a larger amount of clay be used at the fiber optic/specimen interface in order to increase the distance between the fiber optic and cured excess resin.

5.3 Fabrication Method Summary

A wet hand lay up method is a very basic form of composite material fabrication. It is often used at the developmental stages of a composite material design. Embedding a fiber optic sensor into the material is an appropriate means of monitoring the health of the material internally. However, without any precautions taken, the fiber optic can easily be damaged while attempting to extract it from the excess resin surrounding the cured composite. Two methods were attempted to alleviate this problem; the reduced resin method and the clay method. The reduced resin method did not assist with fiber optic

extraction. The clay method was successful in protecting the fiber optic and protective tubing. This method was then further developed. By coating the protective tubing and fiber optic with a high curing temperature clay, the fiber optic is protected from the excess resin surrounding the material. After curing, the clay can easily be removed by hand, leaving the fiber optic intact. The excess resin can then be removed by an appropriate cutting method.

5.4 Specimen Summary

Twelve specimens with embedded fiber optic sensors were fabricated using the method previously defined. The fiber optic was embedded in the center of the specimen longitudinally, as shown in Figure 28

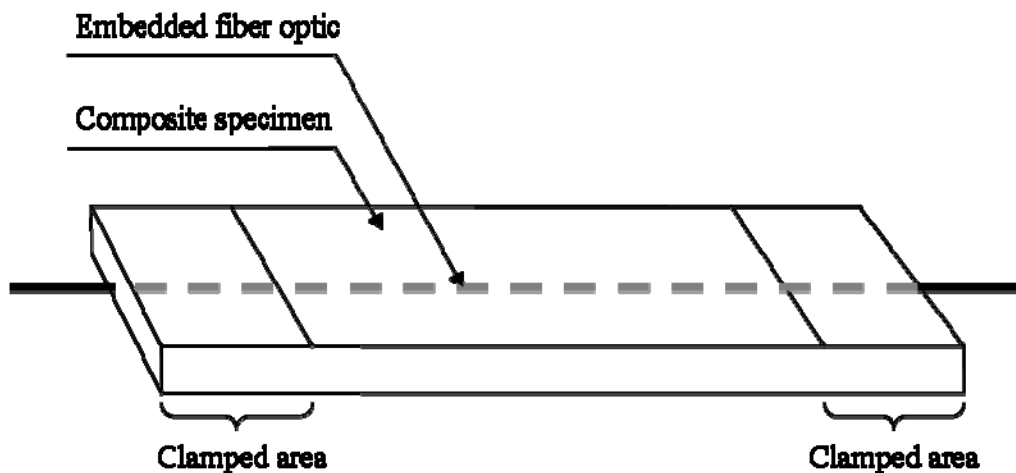


Figure 28 - Desired Specimen Layout

The specimen was designed such that the fiber optic FBG sensors will be sensing the internal behavior of the laminate itself and not any boundary condition issues. The width of the specimen was selected so that edge effects would not be sensed by the fiber optic sensors; such as peel stresses or the initiation of edge delamination. It was also desired to have ample spacing between the first and third sensor from the clamped area of the specimen. The final specimen design is shown in Figure 29.

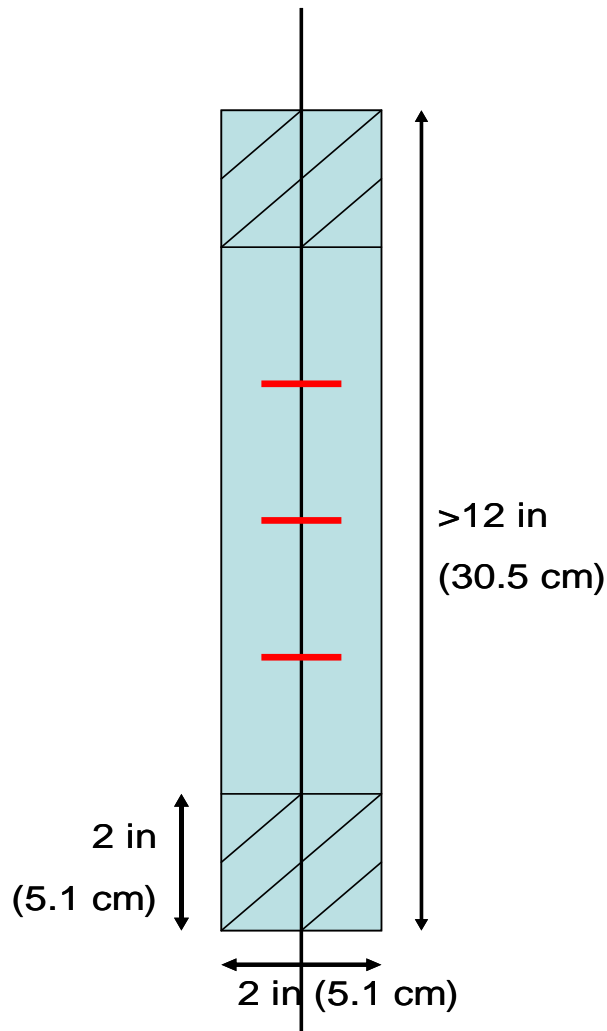


Figure 29 - Specimen Design

Preliminary calculations lead to the surface area that was required to be clamped by the testing fixture. A very conservative estimate was used since the exact effect of the clamping pressure on the fiber optic was not certain. Also, it was important to ensure ample spacing between the end tab plate to be gripped by the test fixture and the embedded protective tubing. Again, since the precise effects of the grip pressure on the fiber optic were not certain, should the protective tubing be embedded in a region that is within the clamped area, there would be an added stress concentration on the fiber optic. Of main concern is where the fiber optic exits the protective tubing within the specimen. Should this additional stress concentration exist, the fiber optic could fracture due to high

shear. Therefore, it was ensured that a portion of the specimen at the fiber exit was not adhered to the end taps as shown in Figure 30.

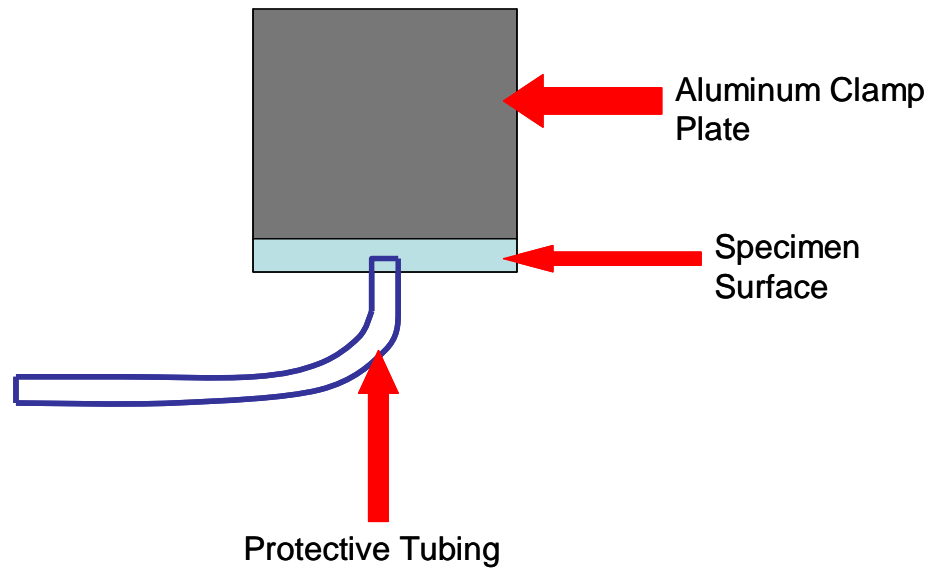


Figure 30 - End of Specimen to be Clamped

Previous testing of the unidirectional specimens with the same constituents revealed the mechanical properties to be that as listed in Table 1.

Specimen Type	Modulus (ksi)	Ultimate Stress (ksi)	Ultimate Strain (%)
C0/C90/C90/C0	7730	125.3	1.621
C0/G90/G90/C0	7266	118.8	1.635

Table 1 – Mechanical Properties from Previous Testing

However, it is suspected that the fiber volume fraction of the specimens fabricated was lower than that of the specimens tested to obtain the above results. Thusly, it is assumed that the fabricated specimens have poorer mechanical properties than the values listed above.

6 Experimentation

6.1 Sensor Selection

6.1.1 Mechanical Resistance Strain Gauges

Strain gauge selection needs to address appropriate size, material, adhesive and mechanical properties. It was initially desired to use strain gauges that could continuously be used to compare its readings with those readings given by the FBG sensors.

There are three main types of material that the resistance grid of the strain gauge can be fabricated from; constantan alloy, isoelastic alloy and karma alloy. Isoelastic alloy gauges are used purely for dynamic strain measurements and are not normally used for static strain measurements [43]. Further, isoelastic alloy is extremely sensitive to temperature changes such that a change in temperature of 1°C will give an apparent strain indication of 300 to 400 $\mu\epsilon$ [44]. Therefore, this material type is not appropriate for this application; leaving constantan and karma alloy.

In further investigating the more appropriate alloy for this application, strain gauge fatigue life was examined. The fatigue limit of karma alloy is higher than that of constantan however, lower than that of isoelastic [44]. Also, the larger the grid area of a gauge, the higher its fatigue life and the higher the gauge's resistance, the lower its fatigue life [45]. The fatigue lives of a variety of gauges, as published by the manufacturer in reference 45, are for strains well below that which is expected to occur. It was therefore concluded that due to the expected strains, any gauge type would not last the duration of the test.

The solder terminals and leadwires connected to the gauge need to be considered when considering the fatigue properties of the entire strain gauge system. The manufacturer

recommends the use of bondable terminals to provide an anchor for the leadwires in order to prevent damage to the gauge when the leadwires are subjected to any type of force [46].

Strain gauges are known to increase in temperature as a result of power dissipation. The power dissipated by the gauge depends on the voltage applied to the gauge and the gauge resistance, as defined by equation 10.

$$P = \frac{V^2}{R} \quad (10)$$

The power is dissipated in the form of heat and the temperature of the gauge must increase above the ambient temperature to dissipate the heat [44]. This is of great concern when applied to a polymer matrix composite material since the polymer matrix is of low conductance. Therefore, the heat generated by the power dissipated from the gauge will increase the temperature of the specimen in the surrounding area. This can then alter the mechanical properties of the specimen in this area and could also possibly damage it. Further, since the gauge is only reading the strain values of the area to which it is affixed, any alterations in the mechanical properties of the material in this area will lead to a non accurate depiction of the material properties and performance as a whole. An increase in temperature would cause the material to deform or elongate, i.e. strain, much easier. Thusly, higher strains would result. Extremely low values of excitation are required to avoid serious self-heating effects.

The modulus of elasticity of the common plastic drops rapidly as temperature rises, increasing viscoelastic effects [47]. Recommendations have been set out to address this very issue [48]. It is recommended that the excitation voltage for the gauge be as small as possible (1 to 2 Volts is recommended) and that the resistance be as high as possible and at least 350 Ω .

The size of the gauge itself is a factor that warrants consideration. The grid must be large enough to encompass a representative area of the material itself. If the gauge is too small

then the strain seen may only be that of the underlying material. This is of most concern upon damage to the specimen as an undamaged specimen should strain uniformly. The larger the gauge however, the lower the power density which is a key variable in the heat dissipation characteristics of a strain gauge [44].

As a result of the factors mention, an ideal selection would be a .25 inch grid, karma alloy 1000 Ω gauge. However, the availability, lead time and cost of this type of gauge are quite substantial. Further, since the gauge was not expected to last the duration of the testing, a more available gauge was selected. Constantan gauges are the most commonly used gauges and was selected. Further, 350 Ω gauges are substantially more common and less costly than 1000 Ω gauges. The gauges used were Vishay Micro-Measurements EA-06-250AE-350, using an excitation voltage of 1.5 volts.

The type of adhesive selected was a two part epoxy. The adhesive was supplied by Vishay Micro-Measurements and is referred to as M-Bond AE-10. This was selected as it has similar properties to the matrix material of the specimen.

Surface preparation for strain gauge bonding onto a composite material is a delicate process as care must be taken to ensure that the underlying material is not damaged. Specifically, damage to the fibers can result in poor material performance in the vicinity of the gauge. Also the surface must be properly cleaned with the appropriate materials to ensure a secure bond between the adhesive and the specimen while at the same time the materials should not react with the specimen. The guidelines given by the manufacture in reference 49 were followed for this process.

Composite materials are orthotropic. Their material properties vary with direction. For this reason, it is especially important to have the strain gauge placed at the proper angle. A variation in gauge placement will corrupt the resulting interpretation of the measurements.

6.1.2 Fiber Bragg Grating Sensors

It is common in the literature to see fiber Bragg grating sensors over 5 mm long. In this instance, a gauge length of 3 mm was selected for two reasons; to see if chirping issues faced by others could be minimized and to begin to investigate the behavior of shorter grating sensors due to their desired use in possible future crack detection projects.

Three gratings were written on each array and placed 2 inches apart; as shown in Figure 31. The spacing was selected so that they were evenly spaced in the specimen with the center grating in the center of the specimen.



Figure 31 - Fiber Optic Array Layout

Three gratings were used to show repeatability in the results; especially the residual stress results. Further, as it was expected that the center of the specimen would experience a larger stiffness drop than the area of the specimen closer to the end tabs; the two sensors close to the end tabs should be in somewhat relative agreement and differ from that of the center sensor.

6.2 Sensor Calibration

In order to ensure functionality and accuracy, both the mechanical resistance strain gauge and the fiber optic sensor needed to be calibrated. Also, this provided an opportunity to compare the strain readings of both sensors to theoretical values. Two calibration methods were used; beam in bending and a tensile specimen test. For the tensile test, the specimen was loaded both elastically and to fracture.

6.2.1 Beam Bending

A beam bending calibration consists of fixing a specimen at one end and displacing the other end a known amount. The applied force, F , can be determined based on the end displacement, δ , the Young's Modulus, E , the moment of inertia, I , and the length of the beam, L , as stated in equation (11).

$$F = \frac{3\delta EI}{L^3} \quad (11)$$

$$\text{Where,} \quad I = \frac{wt^3}{12}$$

With the applied force known, the theoretical stress at any point on the beam can be determined using equation (12); where F is the force applied to the end of the beam, d is the distance from the applied force, c is the distance from the neutral axis of the specimen and I is the moment of inertia of the beam cross section.

$$\sigma_{Theoretical} = \frac{Fdc}{I} \quad (12)$$

With the theoretical stress known, the theoretical strain can be determined. Equation (13) assumes that the stress only exists in the longitudinal direction of the specimen. The widthwise and through thickness stresses are set equal to zero.

$$\varepsilon_{Theoretical} = \frac{\sigma_{Theoretical}(1-\nu^2)}{E} \quad (13)$$

The specimen was 6061 Aluminum. Since the cross section of the specimen was symmetric, the stresses and strains on the top of the specimen would be equal in magnitude to the stress and strains on the bottom of the specimen at the same distance, L , along the specimen. If deflected downward, the top of the specimen would be in tension

and the bottom in compression of the same magnitude. For this reason, a fiber Bragg grating sensor and a mechanical resistance strain gauge were both mounted onto the specimen at the same distance, d ; one was on the bottom and one was on the top as shown in Figure 32.

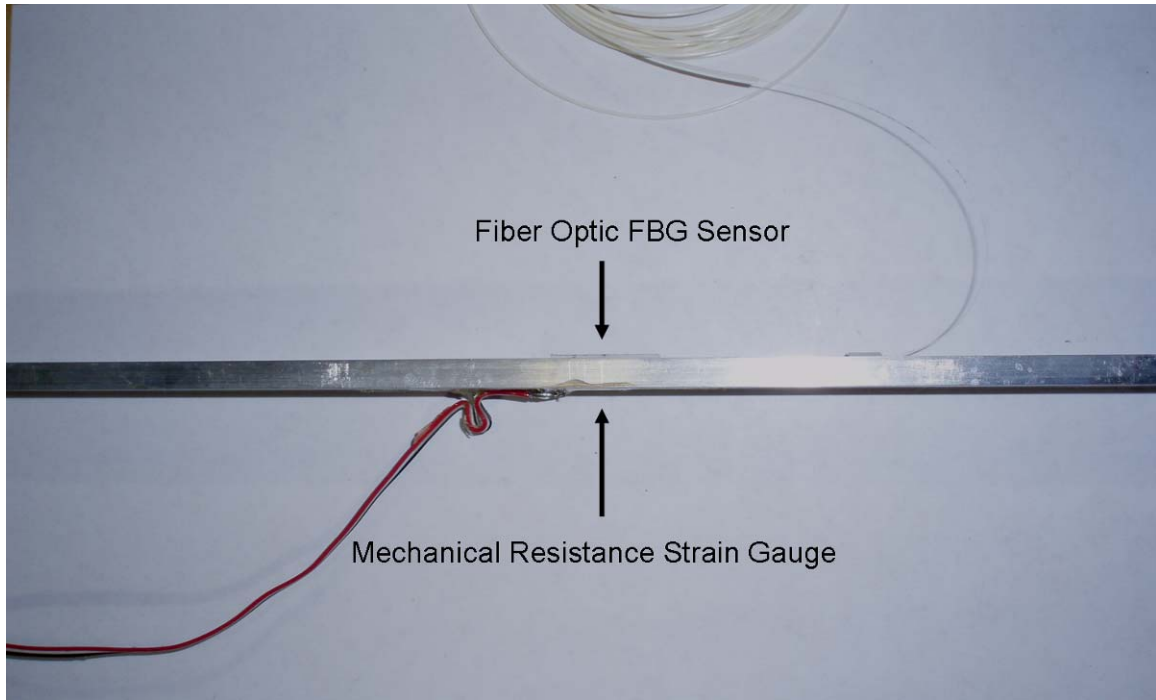


Figure 32 - Beam Bending Calibration Specimen

Once the specimen was secured into the calibration apparatus, the fiber optic was connected to a broad band light source, a coupler and an optical spectrum analyzer as shown in Figure 33.

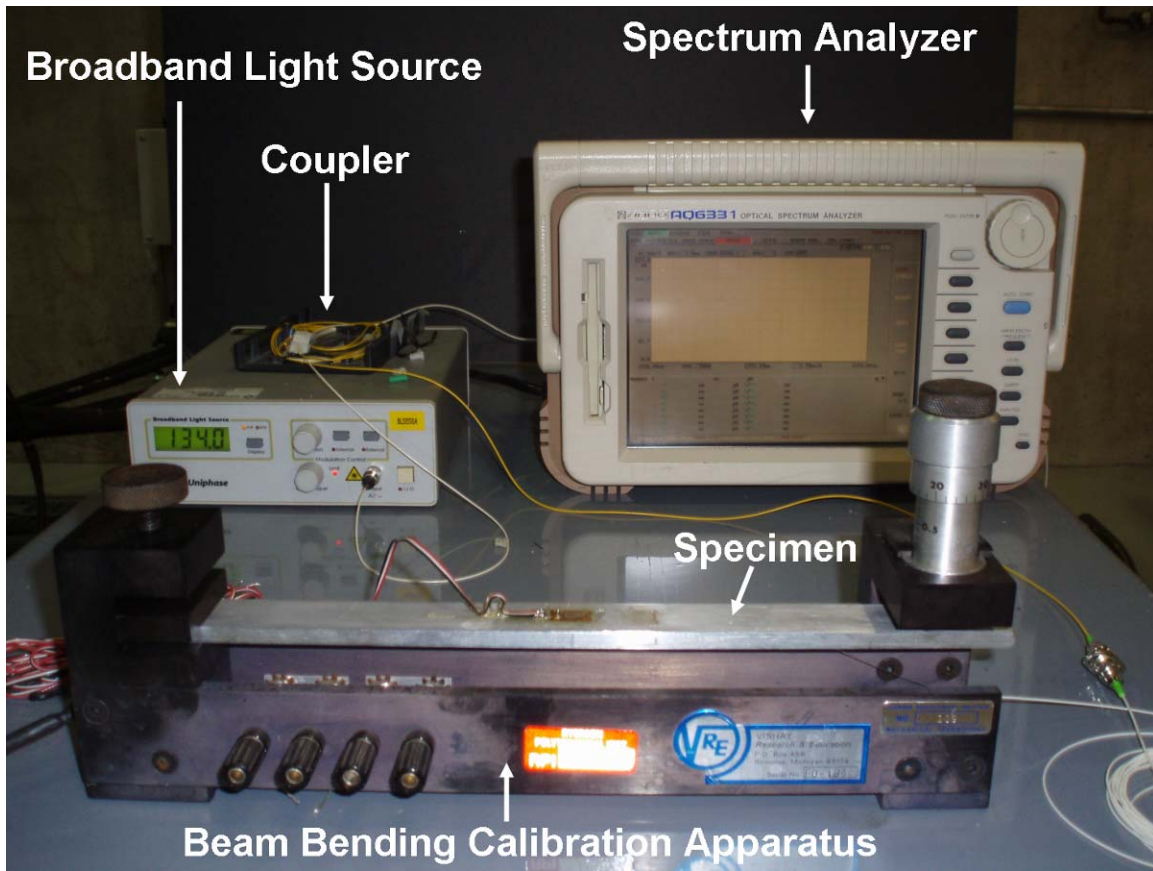


Figure 33 - Beam Bending Calibration Setup

This calibration procedure was conducted over ten times to ensure repeatability and accuracy of the results. The fiber Bragg grating and the mechanical resistance gauge yielded very similar results. The difference between the two strain readings from the two sensors was less than one percent; which is considered to be quite respectable. The percent difference between the theoretical strain and the measured strain was higher at lower displacements than at higher displacements due to measurement sensitivity. At higher displacements and strains over $400 \mu\epsilon$ the percent difference was below 2 % and below 1% at strains over $800 \mu\epsilon$, which is considered acceptable.

Specific calibration attention was given to the fiber Bragg grating alone, to determine an accurate relation between the applied strain and the resulting shift in the peak wavelength. Figure 34 shows this relation to be linear, as expected.

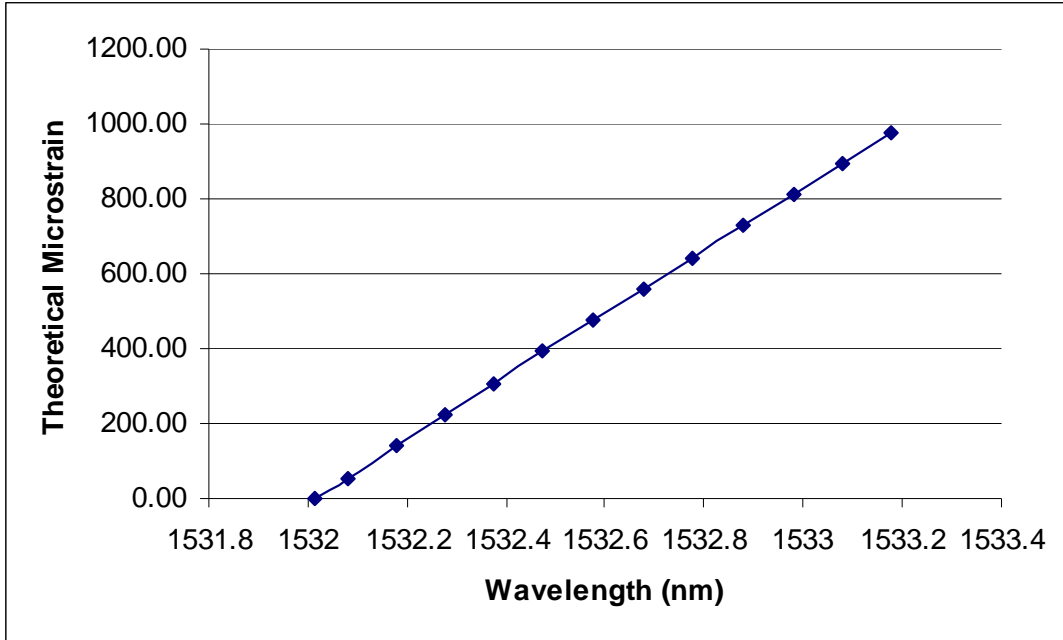


Figure 34 - FBG Calibration Curve (Beam Bending)

Normally, a calibration factor is applied to the wavelength shift directly to determine the resulting microstrain. This factor was calculated and plotted for each calibration run. The results were repeatable and can be seen in Figure 35.

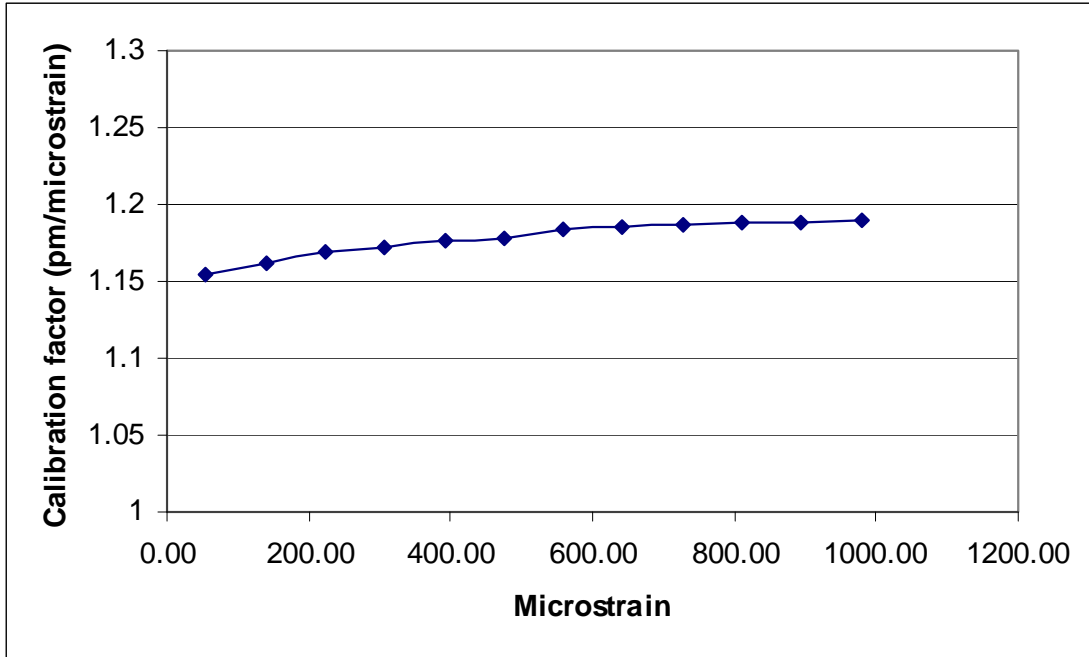


Figure 35 - FBG Calibration Factor (Beam Bending)

It was common to see a lower calibration factor at lower microstrains; however in each instance the results either approached or settled at 1.19 picometers per microstrain. This was the value used in all strain measurements herein. Further, this value is similar to values stated by other researchers.

6.2.2 Tensile Specimen

A tensile 6061 aluminum specimen was outfitted with a mechanical resistant strain gauge and a FBG sensor in the middle of the specimen, each on opposite sides.

6.2.2.1 Elastic Loading

The specimen was elastically loaded in load control so that the load was increased uniformly with time. The load and mechanical resistance strain gauge readings were recorded by the MTS Testware software. The FBG wavelength shifts were recorded by a Micronoptics si425 interrogator. The two sets of data were compared using the recorded timestamps as a reference. Figure 36 shows the two strain gauge readings during the duration of the test.

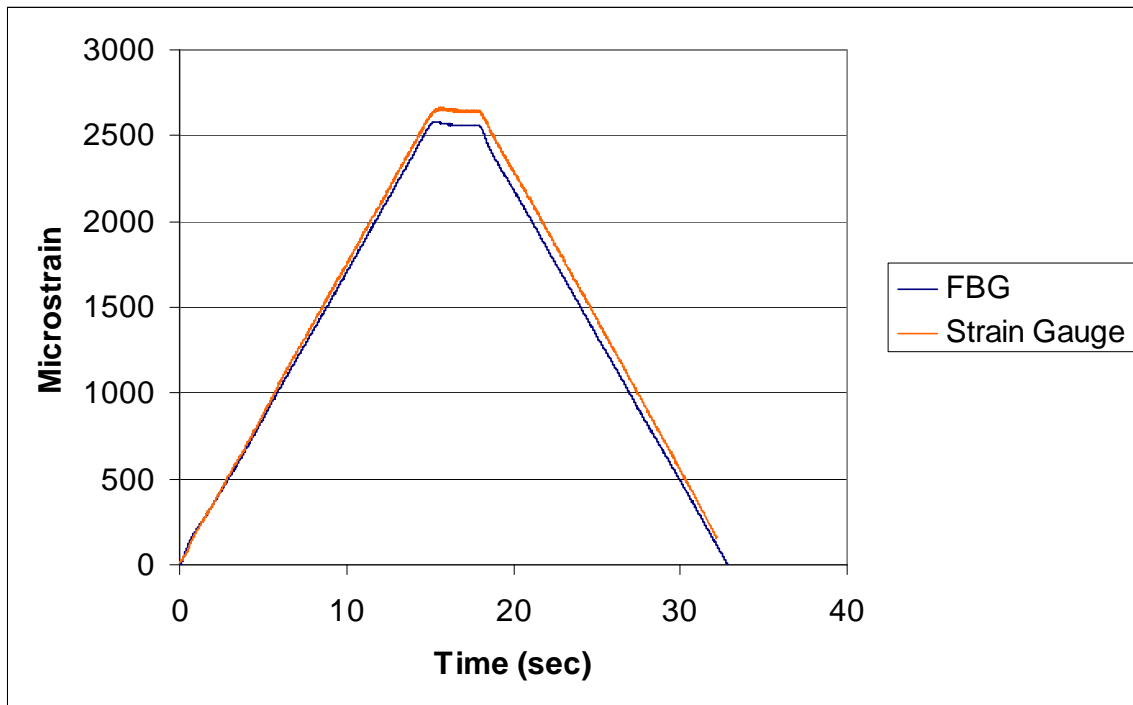


Figure 36 - Gauges Strain Readings with Respect to Time

The microstrain readings from the two gauges are in close agreement with a less than a 4% difference when the load was held constant. The strain readings returned to zero in both cases.

6.2.2.2 Ultimate Loading

The tensile calibration specimen was loaded to the point of fracture. The mechanical resistance strain gauge remained intact. The specimen broke in between the gauge and the solder terminals.

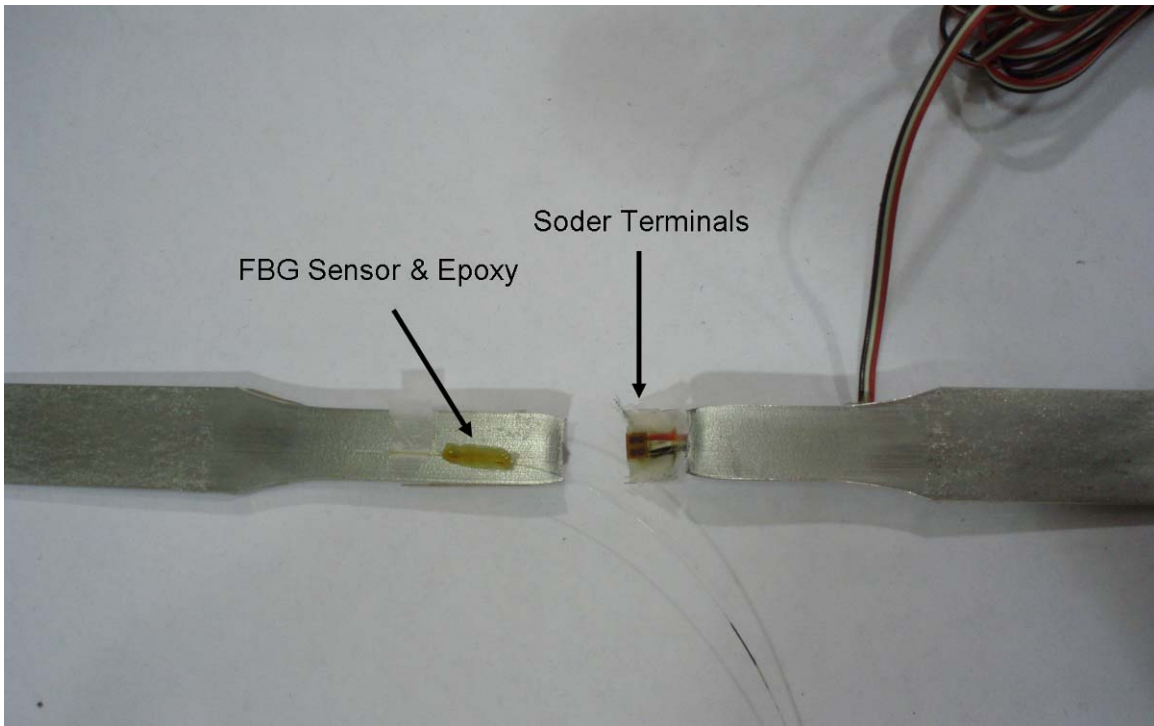


Figure 37 - Tensile Specimen

The fiber optic did not fracture. Rather, the epoxy that adhered the FBG to the specimen debonded from the specimen. This can be seen in Figure 38. In the figure the fiber optic is held onto the specimen with tape at the end.

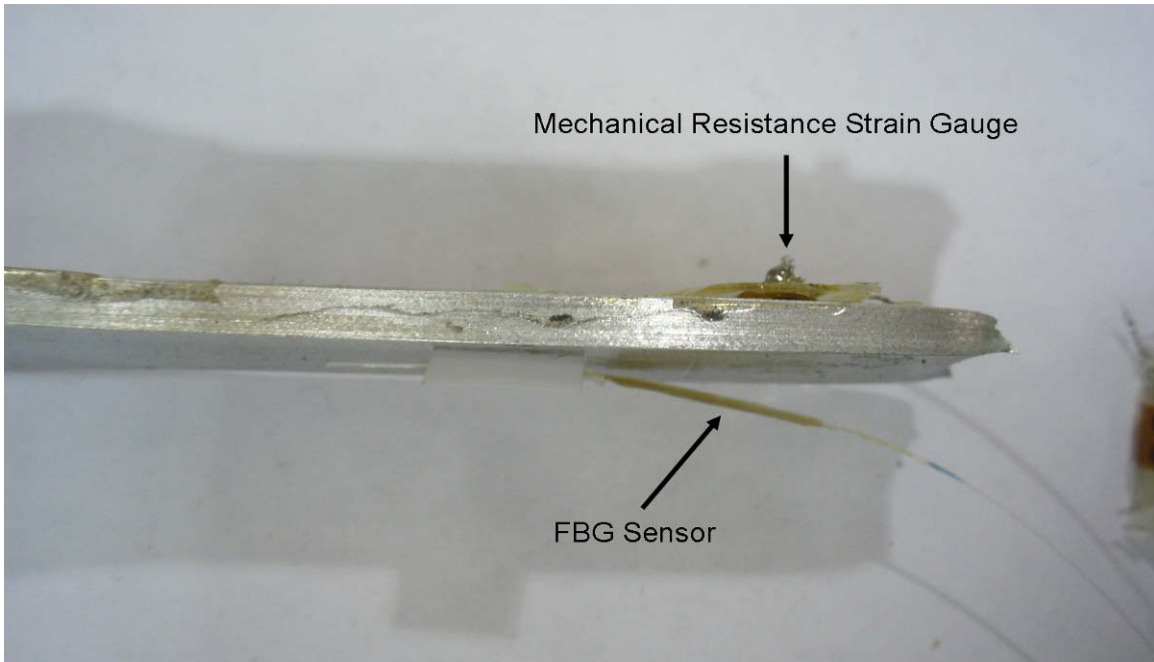


Figure 38 - Debonded Strain Gauges

The ultimate strength of the fiber itself was not determined via testing, however this was not deemed to be necessary as published values of the ultimate strength of fiber optics are higher than the loads expected in further testing.

6.3 *Embedded Fiber*

6.3.1 Wavelength Spectrums

Prior to the embedding of the fiber optic FBG arrays, the freestate reflection wavelength spectrums were recorded. It was necessary to record the initial peak wavelength values so that after embedment, the peak wavelength shift could be determined. It was desired to determine the shift in peak wavelengths to determine the resulting residual stress of the material; which is discussed further in the next section.

Rather than just recording the peak wavelength values, the entire reflection spectrums were recorded both before and after embedment. The direct change in the spectrums can be seen in Figure 39.

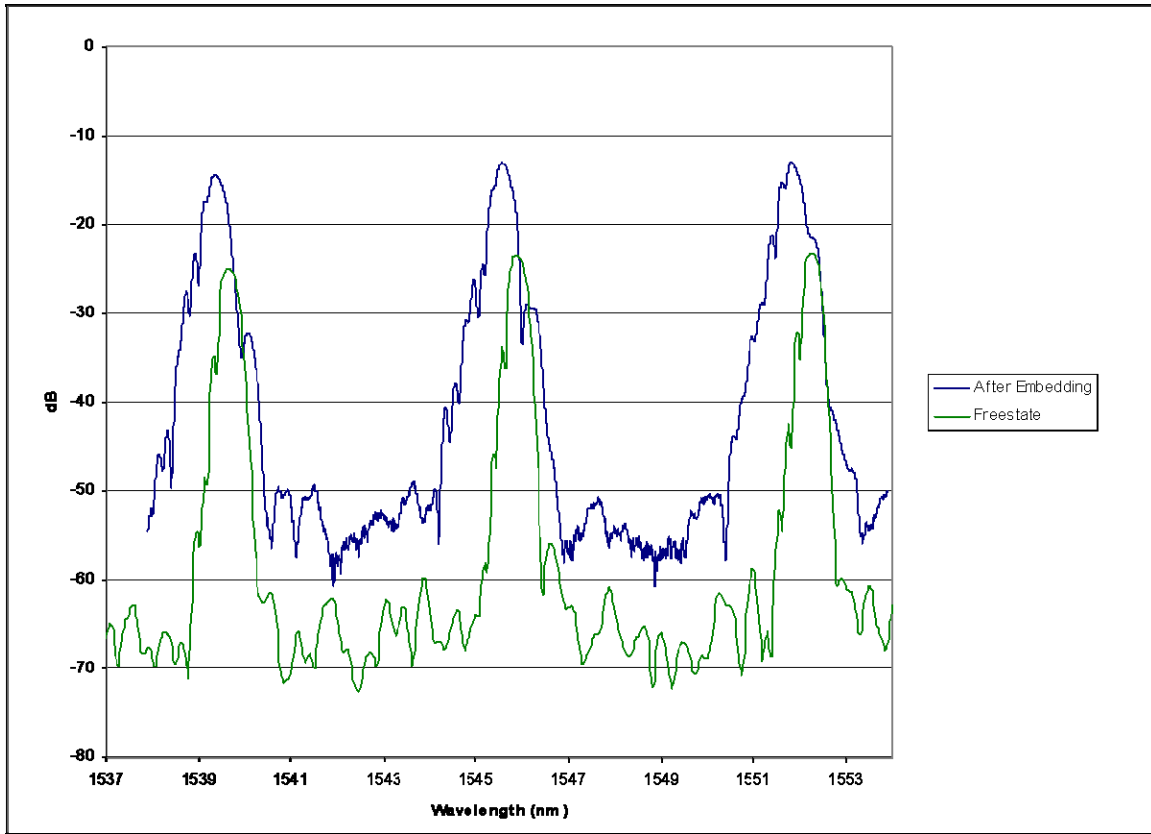


Figure 39 - Change in Reflected Wavelengths of Embedded Fiber Optic Array

From this data it is apparent that the FBGs are now in a state of compression as the peak wavelength values have all decreased. However, it is difficult to assess if there are other immediate differences in the spectrums as they do not have similar reference lines in this depiction. It is for that reason that Figure 40 was created.

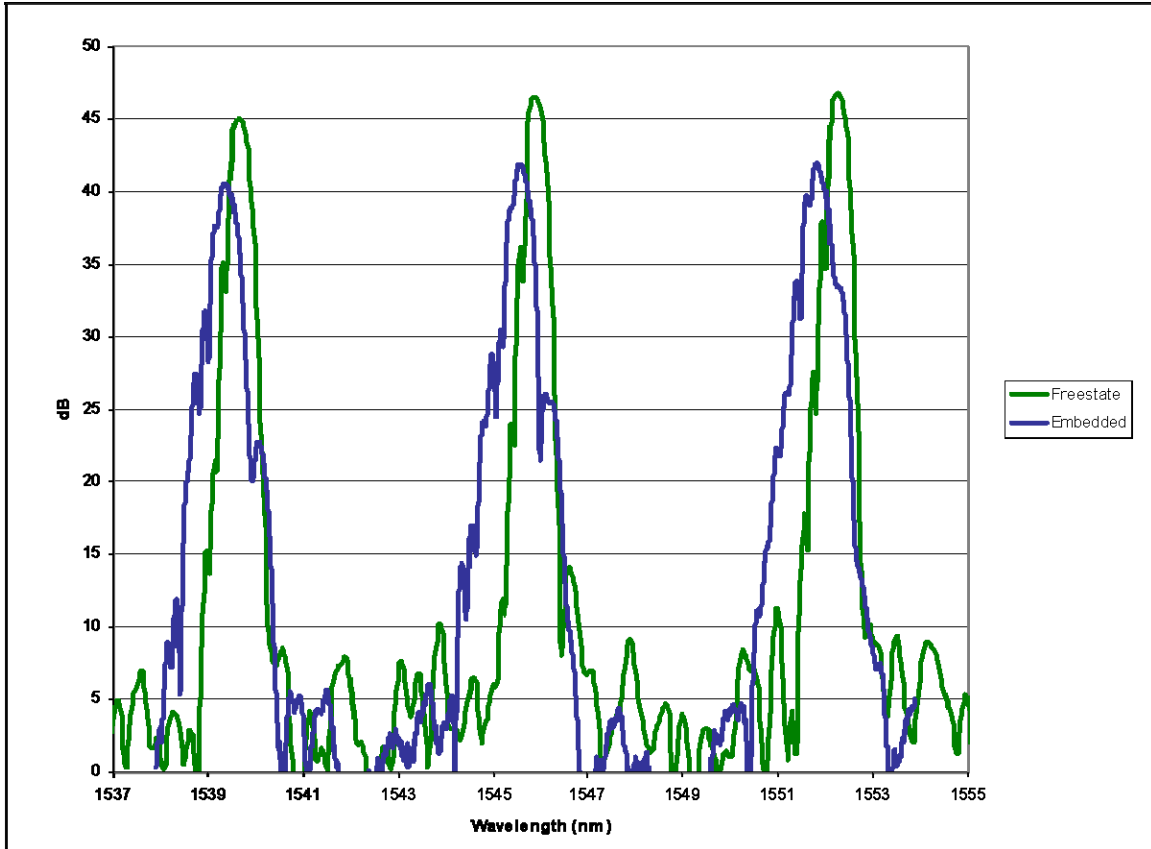


Figure 40 - Freestate and Embedded Spectrums with Same Reference Line

It is now more apparent that the reflected spectrum has decreased in intensity after embedment by approximately 5 dB. This was the average drop in intensity for all the specimens. There is also a noticeable widening in the reflected peaks.

The peaks are not as smooth as they were initially. This is because the peaks have become slightly chirped, due to non uniform strain distributions.

The resulting change in the reflected spectrum is similar in nature to those found and reported by other researchers [39, 40 & 41].

6.3.2 Residual Stress evaluation

The average peak wavelengths were determined for both before and after embedding the fiber optic arrays into the material. The resulting sensed strain was determined. The measured residual strains are listed in Table 2.

Specimen Type	Mean Measured Residual Strain ($\mu\epsilon$)	Standard Deviation
Carbon / Carbon	-314.2	48.1
Carbon / Glass	-325.6	65.6

Table 2 - Specimen Residual Strains

These values were considered appropriate and it should be noted that further statistical analysis was not conducted due to variations in the material. Such analysis would not be purely reflective of the FBG reading. If such analysis is desired it would be necessary to determine variations between specimens independently of the residual strain readings from the FBGs in order to isolate the FBGs accuracy.

Theoretical values were not calculated however due to complexity of modeling and the lack of property information; such as the glass transition temperature, GTT, of the resin. Further, it was the main goal of the collaborating researchers to determine an estimation and comparison of the residual strains, rather than the exact value.

6.4 Tensile Testing

The unidirectional carbon specimens were tested further. Firstly, the undamaged Youngs modulus of each specimen was determined. The fiber optic was connected to a broadband light source and spectrum analyzer via a coupler. This equipment was set up on the test bed of the MTS 322 test frame used. The testing setup used is shown in Figure 41.

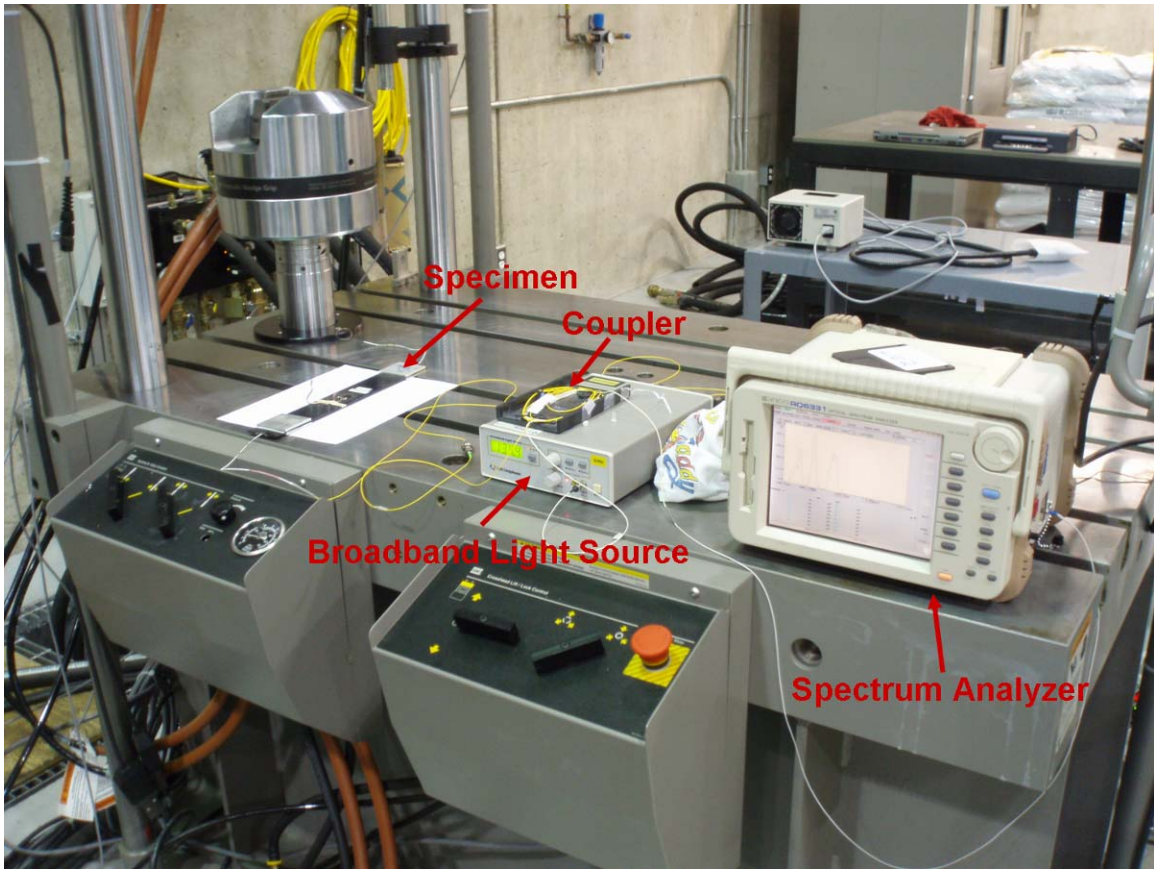


Figure 41 - Test Setup

To determine the modulus, the entire reflected spectrum was recorded. Since most peaks were chirped it was necessary to determine the average peak wavelength. This was done by determining the wavelength at half of the optical power of the peak on each side of the peak and then averaging these values. It was necessary to interpolate between data points for this purpose.

Each specimen was loaded and the load was held constant while the reflected spectrum was measured and recorded. The resulting modulus is then the slope of the stress vs. strain curve. Although only two test points were needed to determine the modulus, at least three were used to ensure validity. An example of the spectrum changes during loading for one of the specimens can be seen in Figure 42.

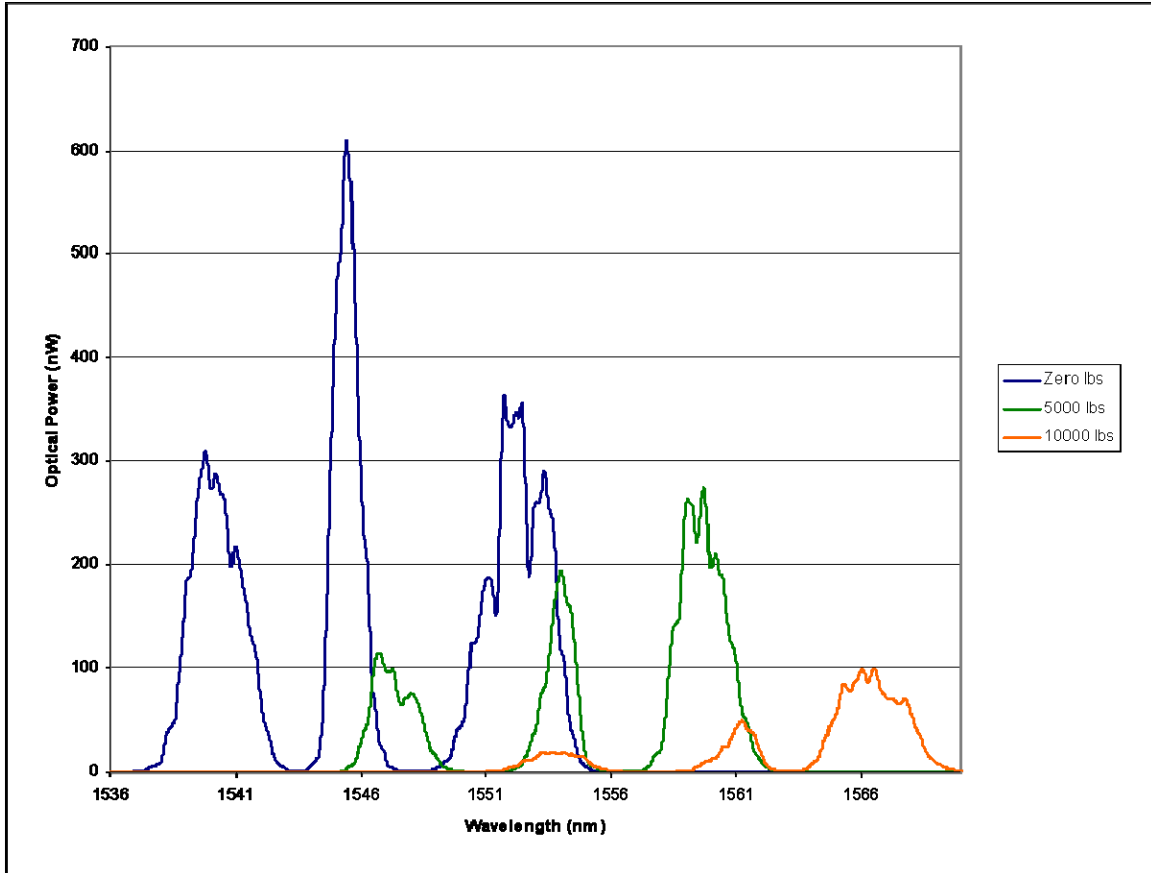


Figure 42 - Spectrum Changes During Loading

As the loading increases, the width of the peak increases and the peak optical power decreases. This behavior is similar to the behavior observed after the fiber was embedded.

Using the average peak wavelength, the specimen stiffness sensed by the FBGs was calculated. Each specimen also had a mechanical resistance strain gauge adhered to the center of the specimen. Based on the loading, and hence the stress on the specimen, and the strain sensed by the gauges; the resulting moduli of the specimens were found. They are listed in Table 3.

Specimen Number	Modulus (ksi)			
	Strain Gauge	FBG 1	FBG 2	FBG 3
1	7120	7900	6717	7137
2	6977	6880	7136	6987
3	6573	6544	6592	6768
4	6606	6492	6662	6692

Table 3 - Initial Specimen Moduli

The alignment and location of the gauges are considered to be the main cause of variation of the initial modulus readings. Also, due to the nature of the manufacturing process used, the material has variations not theoretically expected; such as fibers not completely aligned.

The wavelength spectrum of a specimen with an 8000 lb load on it, which was loaded twice prior, is shown in Figure 43.

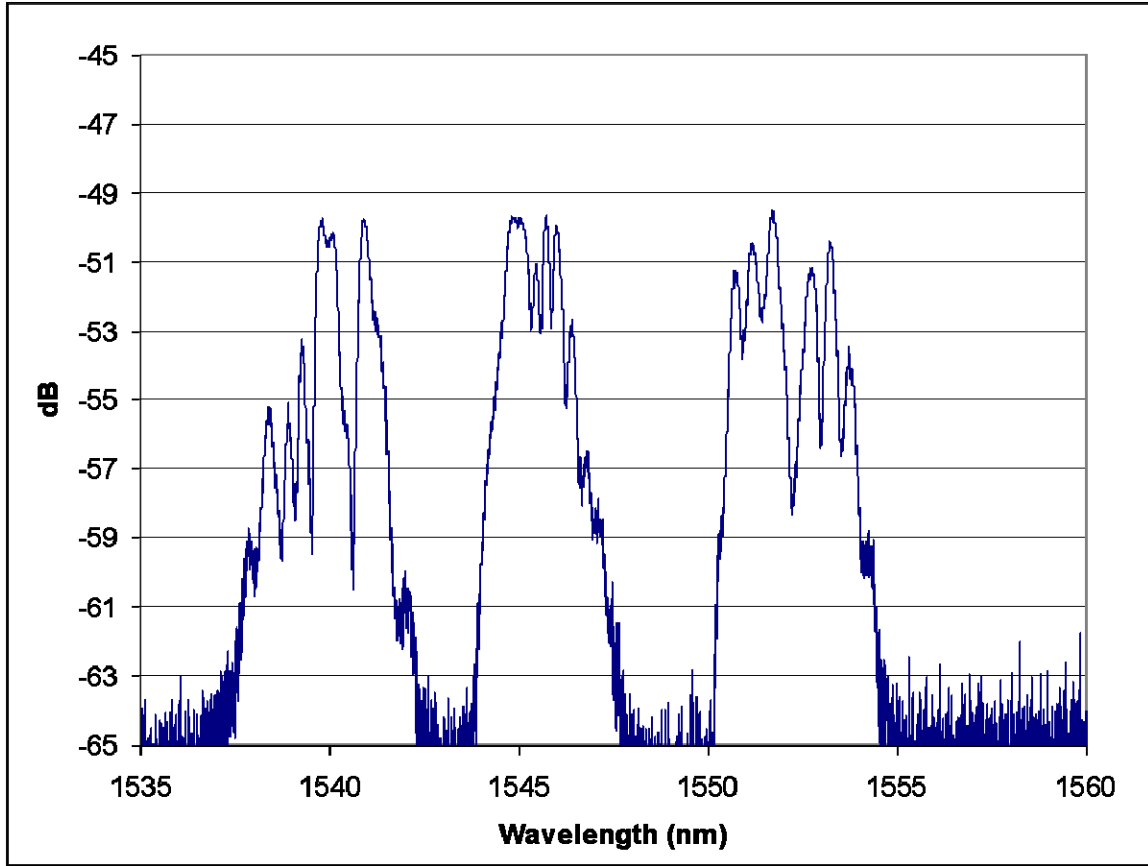


Figure 43 - Highly Chirped Spectrum

This figure is illustrative of the difficulty that can arise from using a peak detection device or an algorithm to detect the peak wavelength for this type of application. The sensors are subjected to non-uniform strain distributions. As the specimen has already been loaded, damage is beginning to accumulate around the FBG sensors. Further illustration of damage accumulation after initial loading is depicted in Figure 44.

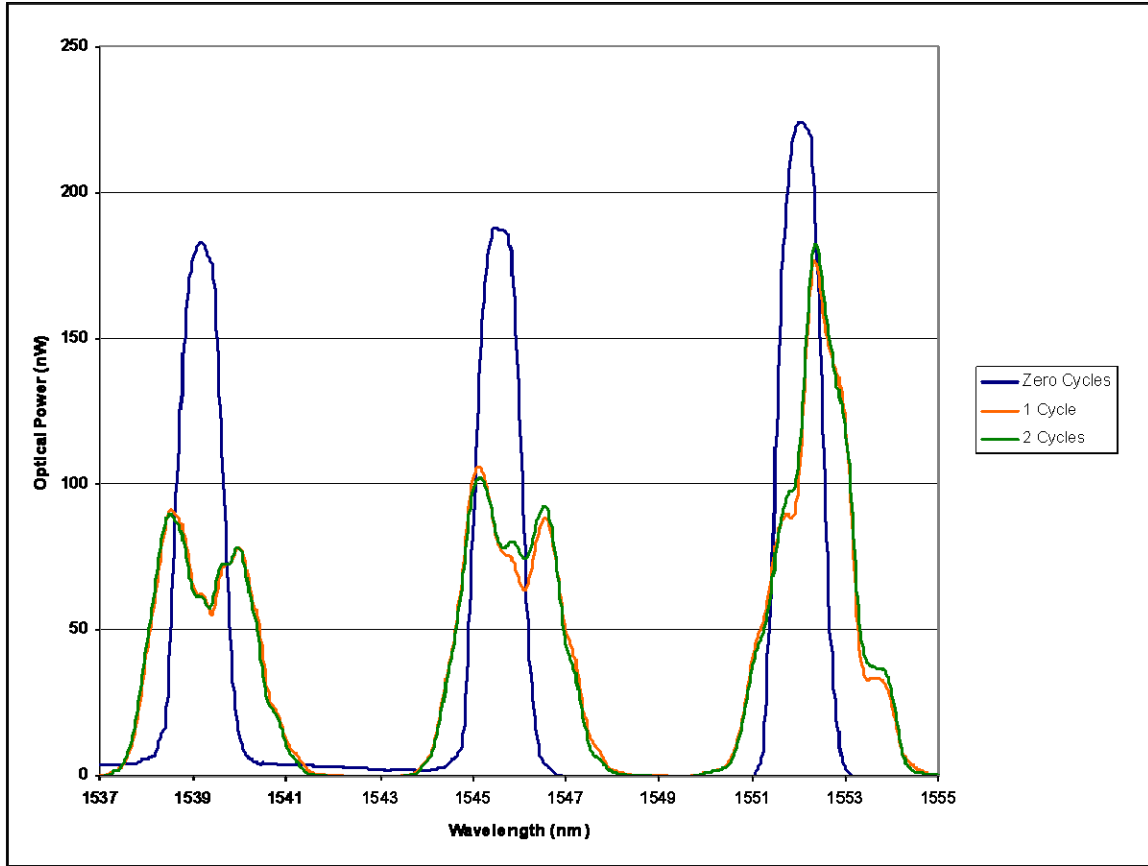


Figure 44 - Damage Accumulation from Initial Loading

Matrix cracking in the vicinity of the gratings is the suspected reason for this chirping behavior. During the initial loading, cracking could be heard coming from the specimen.

6.5 Fatigue Testing

With the initial measured moduli of the specimens determined, the specimens were then subjected to fatigue testing. The specimens were all cycled at a stress ratio of 0.1; which is the ratio of the minimum stress to the maximum stress. The maximum stress values varied with each specimen in an attempt to observe differing behaviors and fractures.

Prior to commencing testing of the specimens, a preliminary specimen was tested to validate the process and insure system integrity.

6.5.1 Preliminary Testing

Preliminary specimens were cut from a carbon/glass hybrid composite that was fabricated during fiber embedment experimentation. The purpose of these specimens was to confirm the integrity of the testing system as well as confirm the test plan. One specimen was used for a tensile test trial and another one was used for a fatigue test trial. These specimens, after testing, are shown in Figure 45. Also shown in the figure is a specimen of the same material that was not used for testing. This specimen has an intact fiber optic embedded in the center of the lamina that can be seen through the glass bundles.

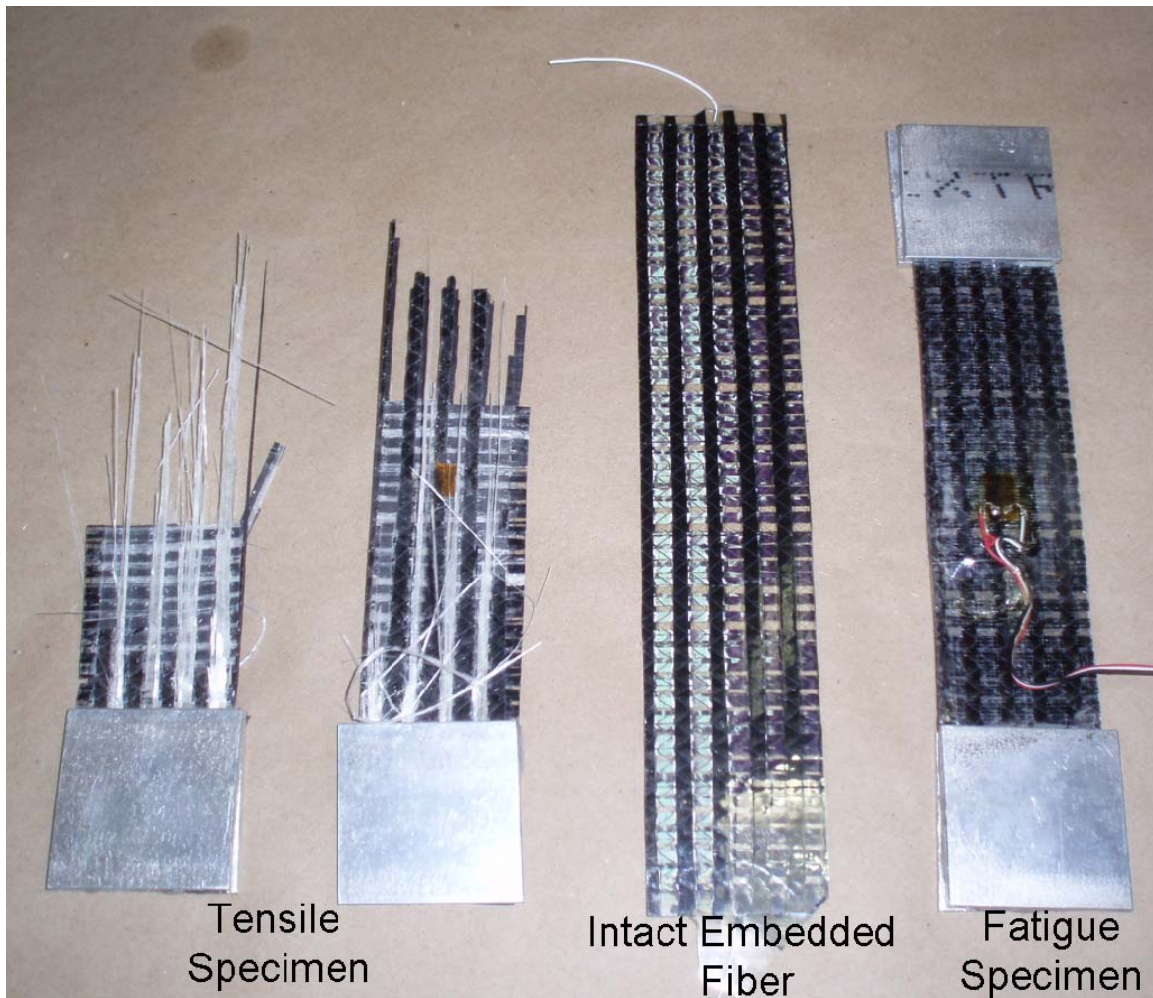


Figure 45 - Preliminary Specimens

Both test specimens were outfitted with a strain gauge. The tensile specimen was the first specimen tested. The glass bundles in the longitudinal direction failed prior to the carbon bundles; which was expected since carbon has a higher ultimate strain than glass. This test was conducted prior to the tensile testing summarized in the previous section, however is mentioned here for completeness.

The fatigue specimen served useful as a means to estimate appropriate cyclic loads for future specimens. The specimen was cycled half a million times with a maximum load that increased throughout the test.

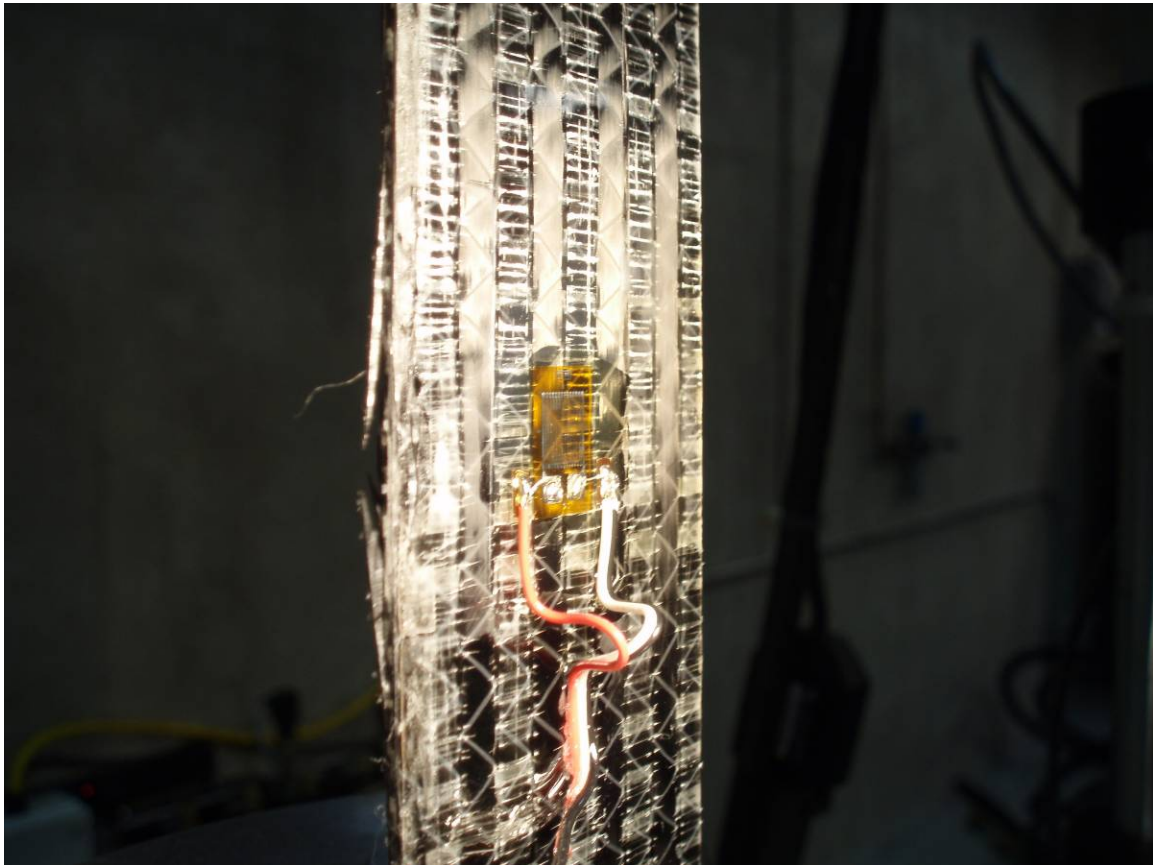


Figure 46 - Preliminary Fatigue Specimen

During the testing, damage accumulation was observed. An example of the observed damage accumulation can be seen in Figure 47.

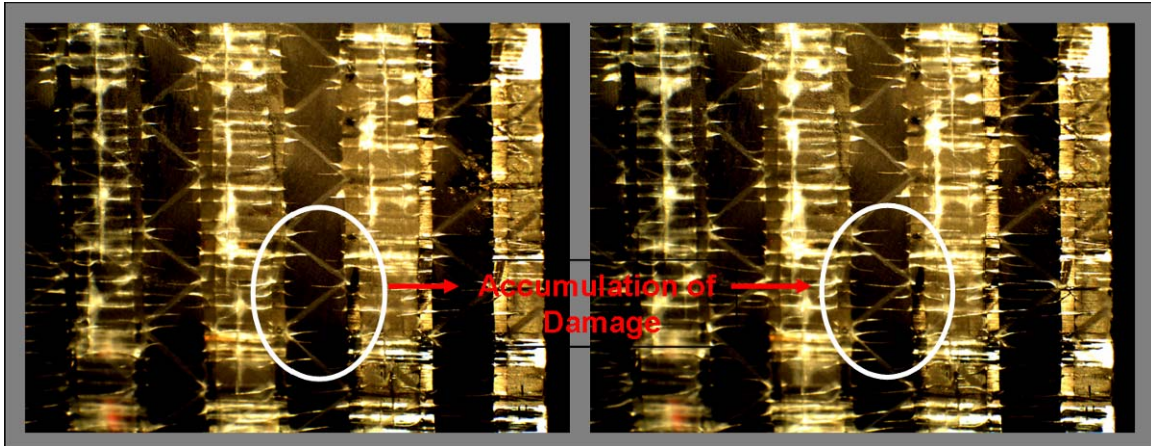


Figure 47 - Preliminary Specimen Damage Accumulation

Of interest was the fact that more damage could be observed in the center layers. This was possible due to the transparent glass bundles in the top layer. The center layers had unidirectional fibers in the 90° direction. This was an expected observation as the center layer was matrix dominated due to the fiber direction and the loading direction. Damage to the strain gauge was also observed. The gauge did not debond and the solder tabs and leadwires remained intact. However, cracks appeared on the foil gauge itself.

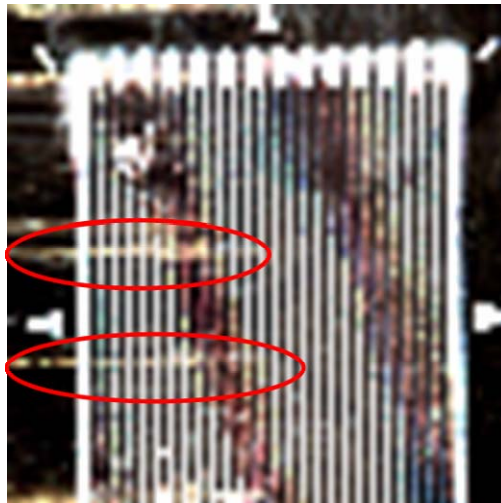


Figure 48 - Cracks in Strain Gauge

The gauge failed prior to any drop in stiffness of the composite specimen. This was an important observation as use of the gauges for a stiffness detection of future specimens

could not be relied upon if the gauges themselves were to be cycled; which would be the case here.

6.5.2 Low Cycle Fatigue

Three of the four specimens were cycled less than one million times. Two of these specimens fractured during testing at less than 100,000 cycles. One of these specimens had a fiber optic that fractured during initial testing. Only one of the FBGs of this damaged fiber optic returned a peak wavelength. However, this wavelength did indicate a drop in stiffness with increased cycles. The remaining specimen was cycled 200,000 times; however the test was interrupted and not carried out to fracture. Prior to test interruption, a drop in specimen stiffness was detected by the FBG sensors.

Figure 49 shows the resulting drop in stiffness detected by the FBGs for a specimen that was cycled to a maximum load of 11,500 lbs. This specimen fractured during the fatigue cycling after the 50,000 cycle readings were taken.

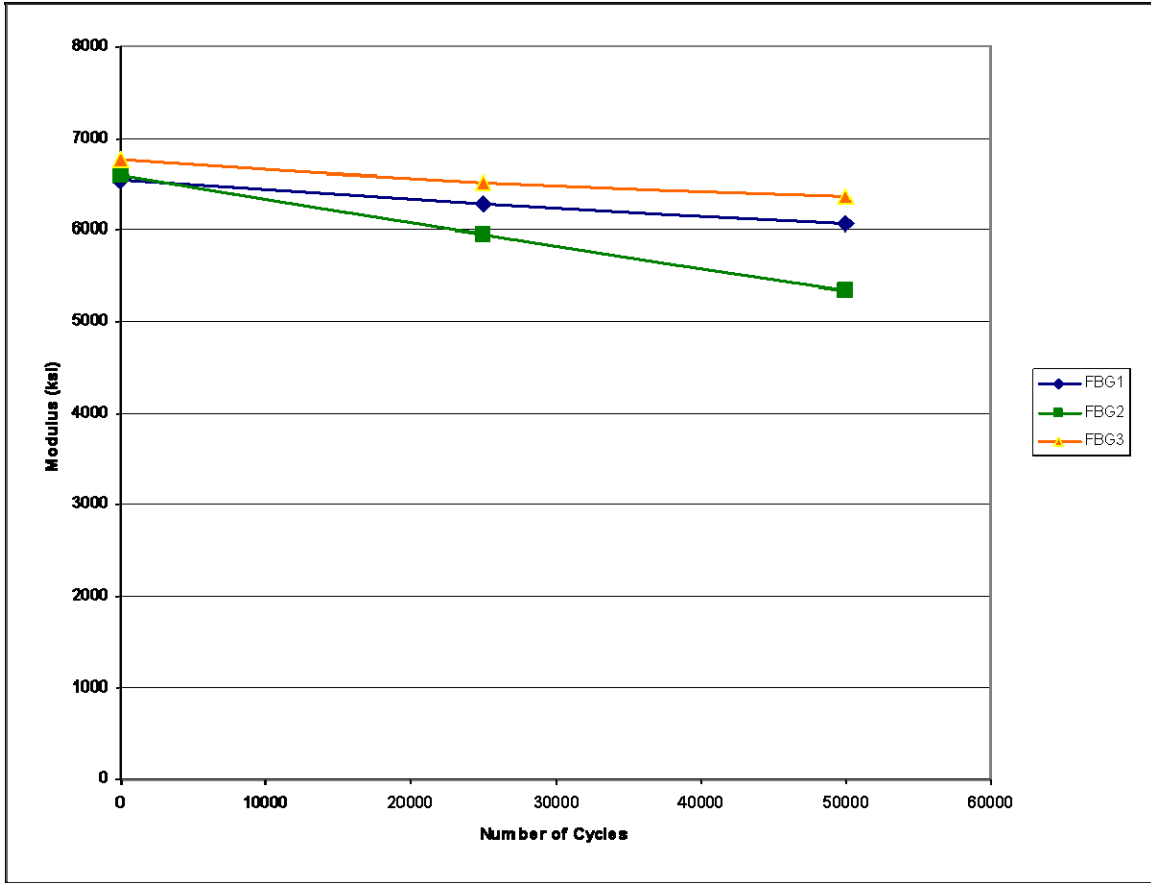


Figure 49 - Drop in Modulus

To better quantify the drop in stiffness sensed, Figure 50 was created. This graph indicates the potential of using embedded FBGs to determine linear damage factors for the stiffness drop in cyclically loaded composite materials.

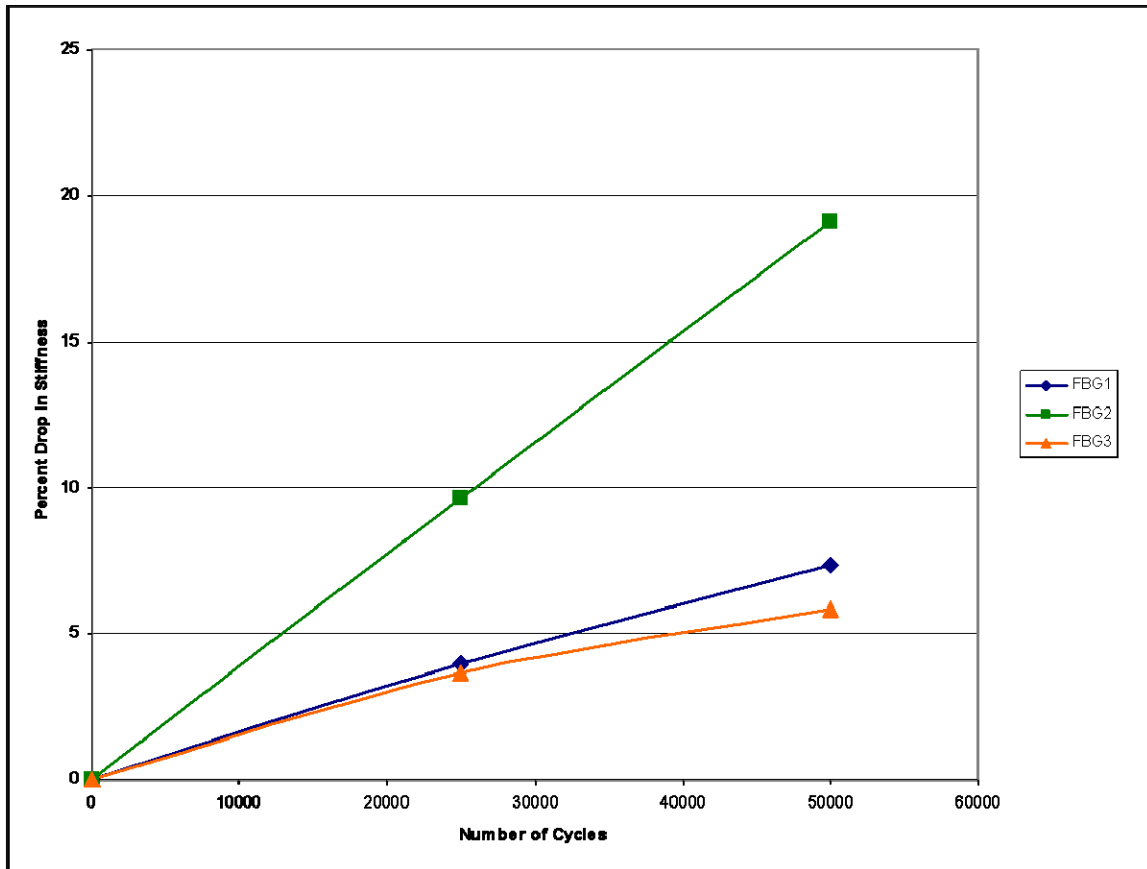


Figure 50 - Percent Drop in Stiffness

Although each specimen indicated that the FBG sensors were capable of detecting drops in stiffness of the material, the results of the other two specimen were not as linear as the results shown here. However, this may be due to specimen variations. Regardless, the results shown here are a promising advance in the development of embedded FBG sensors since this ability has not yet been demonstrated in the literature on a quantitative level. Qualitative fatigue damage detection capabilities have been demonstrated and are present in the literature [40 & 41].

Some visual forms of damaged varied between specimens. It was common to see fibers at the edges of the specimen debond from the specimen; most likely due to the fact that cutting of the specimens cut some of the longitudinal fibers. Delamination buckling was also witnessed, as shown in Figure 51.

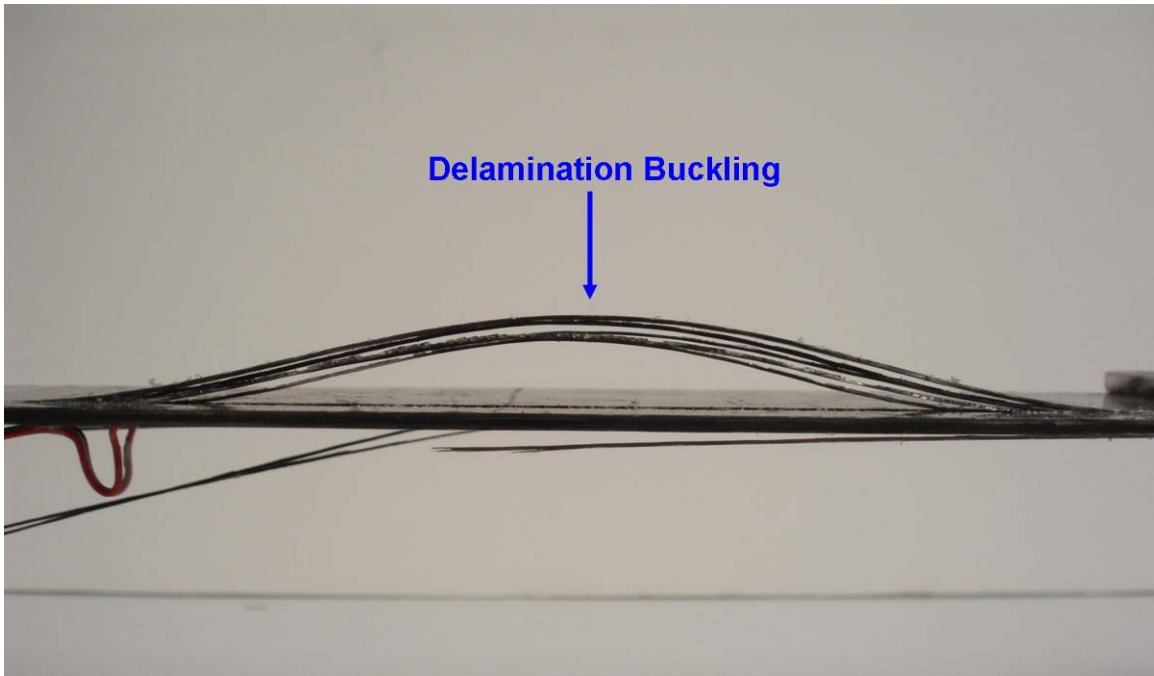


Figure 51 - Delamination Buckling

This observation is further validation of the compressive residual strains measured.

The final fracturing of the specimen was quite violent in nature and occurred quite suddenly. Fracturing noises could be heard prior to the final fracturing however, these noises did not coincide with any major visual indication of damage. Upon final fracture, the specimen separated into multiple pieces and scattered around the test fixture. The remains of the specimen left in the fixture can be seen in Figure 52.

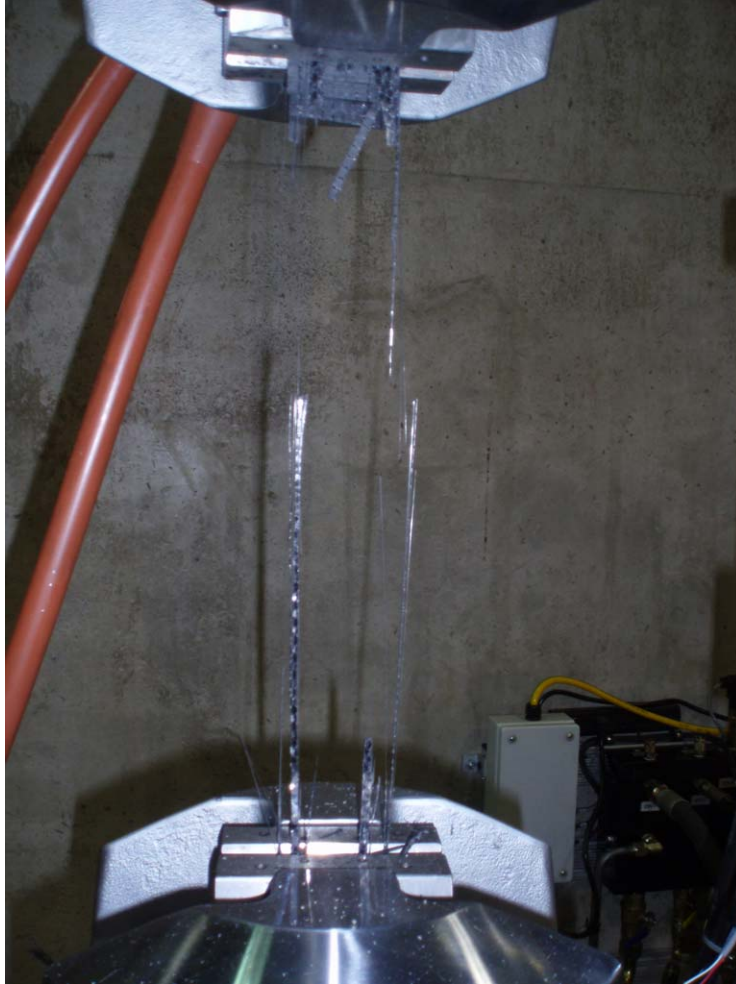


Figure 52 - After Specimen Fracture

By all indications, the FBG sensors appeared to be functional up until fracture.

6.5.3 High Cycle Fatigue

One of the specimens was cycled one million times; with a maximum load of 10,000 lbs and a stress ratio of 0.1. However, prior to any initial loading the reflected spectrum appeared as though it might have been damaged. The wavelength peaks could be determined, however where it was expected that the optical power should have been zero, or relatively close to zero (i.e. non peak values) there did exist a significant amount of optical power.

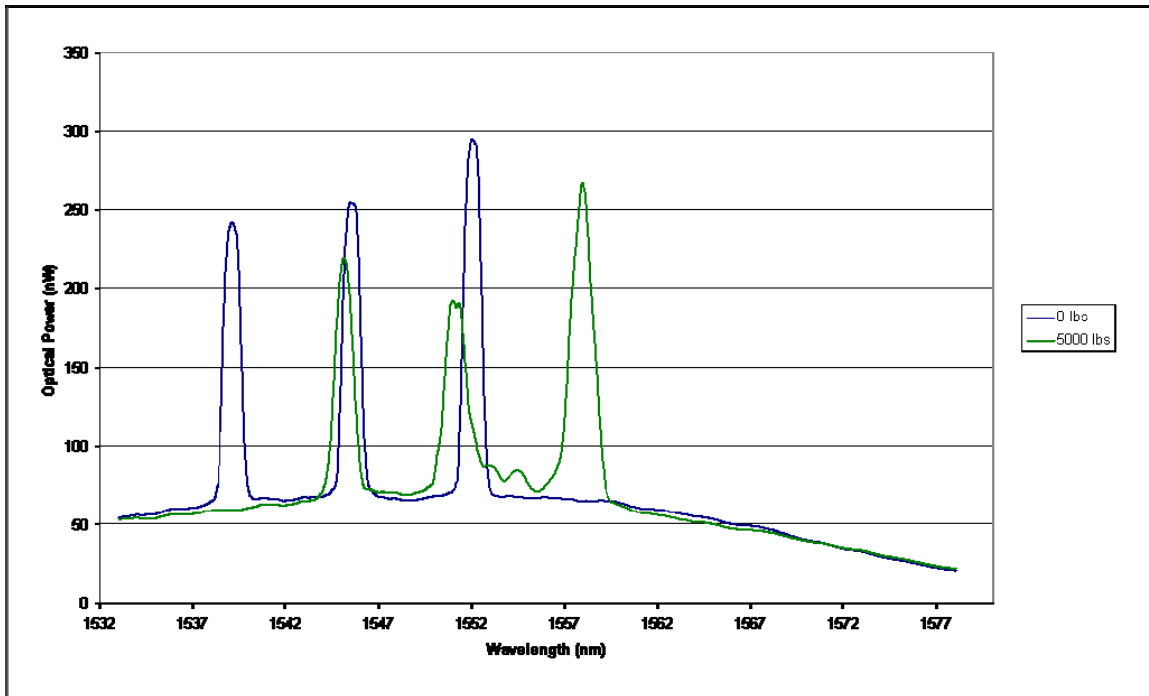


Figure 53 - Portion of Entire Light Spectrum Reflected

Based on the shape and consistency of the resulting baseline, it can be concluded that a portion of the entire light spectrum is being reflected. Of interest to note is that when the reflection spectrum was measured just over one month prior, this portion of the light spectrum was not being reflected. During the time that had elapsed, this specimen was stored, treated and outfitted with a strain gauge in the same manner as the other specimens; none of which displayed similar behavior.

To compensate for this, an average value for the baseline optical power for each wavelength was determined. This value was then subtracted from all the readings to mimic a zero baseline value. This was done to assist in proper determination of peak values but more importantly, since the half optical power bandwidth would be skewed as a result of the sloped baseline values and the fact that there is considerable width to the peaks themselves.

A further development occurred later in the testing as the FBGs exhibited unexpected behavior between 325,000 and 350,000 cycles. The peaks appeared to have merged and

never returned to their original behavior. Figure 54 shows the reflection spectrum with no load placed on the specimen.

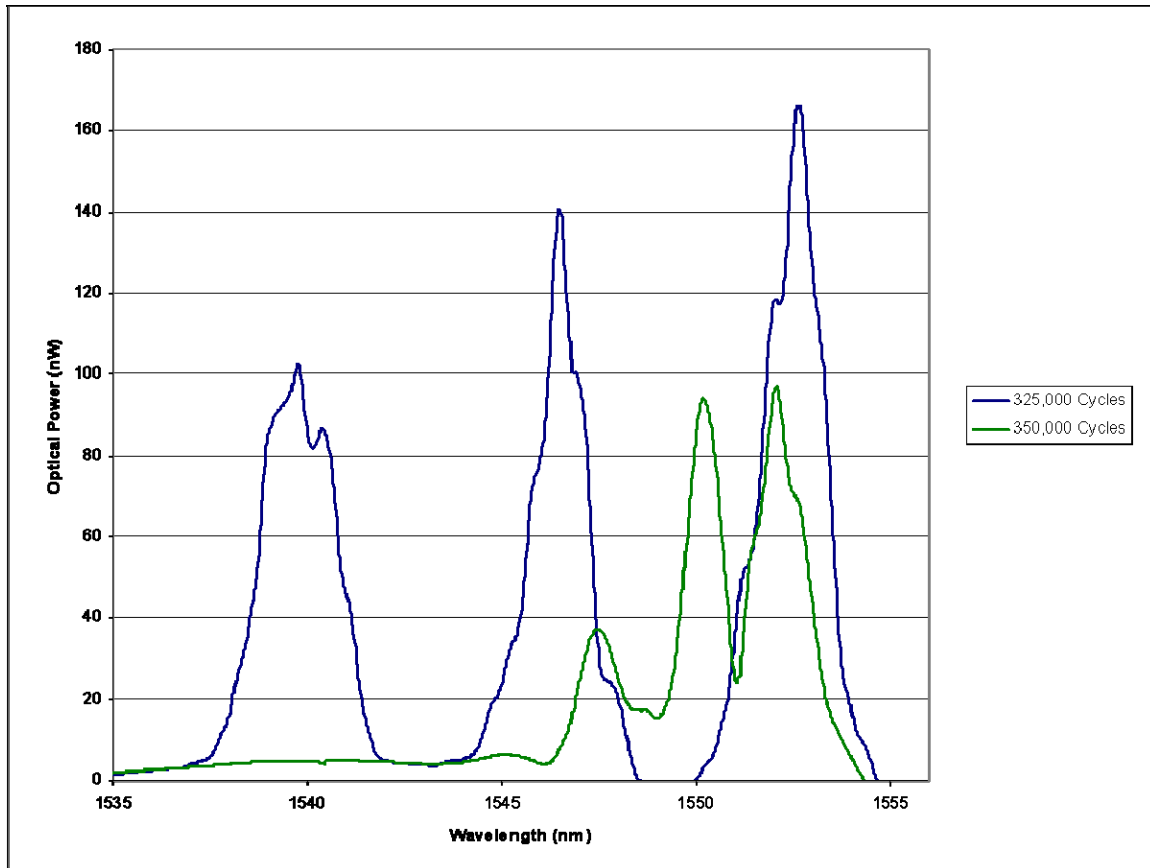


Figure 54 - Zero Load Reflection Spectrum

Prior data leads to the expectation of a very small shift and/or change in the reflection spectrum than what is seen here.

Although the specimen was tested further, the data obtained cannot be trusted to be accurate since the fiber is damaged. Further, since this all occurred prior to one million cycles, no conclusions can be made on the high cycle behavior of the fiber optic. It is possible that this specimen is a damaged anomaly. However, the data collected in the beginning of the cycling showed similar results to that obtained by the other specimens; that an initial drop in stiffness and damage detection in the vicinity of the FBG can be detected.

6.6 Further Discussion

Loading of the specimen introduced matrix cracking mainly in the center layers of the specimen. The center layers were matrix dominated as the fiber bundles are perpendicular to the direction of loading. Therefore, it is expected that high loads will initiate matrix cracking. Further, the resulting reflected spectrum became chirped upon loading. This further confirms a non uniform strain field in the vicinity of the FBG due to matrix damage. This observation of change in the reflected spectrum upon internal damage is consistent with observations made and commented on in the literature [39, 40 & 41].

The exact location of the grating is uncertain. Further, it is not known if each grating is in a similar location. One grating may be in a matrix rich region whereas another grating may be in a location dominated by the fibers. Further, it is even possible that the grating may be directly influenced by the fibers in the longitudinal direction of the specimen. Figure 55 is a picture of the cross section of the specimen. The dark zig-zag region in the center of the specimen is where the fiber optic was located.

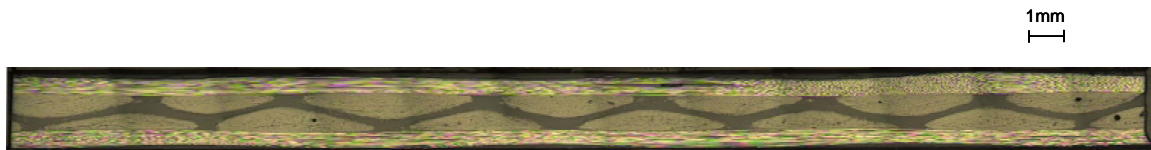


Figure 55 - Specimen Longitudinal Cross Section

As can be seen, there is much variation as to where the gratings could be located.

As previously mentioned, it is accepted that the fiber optic poses no degrading effect on the host material should the fiber be placed in the direction of the fiber bundles. The opposite is the case with these specimens as the fiber was placed perpendicularly. This can be considered to be a harsher environment for the fiber optic to endure due to the load carried by the fiber compared to that of the surrounding material. Further,

perpendicular matrix cracking can introduce localized shear stresses surrounding the fiber at the matrix crack tips. As the surrounding matrix material cracks propagate, the fiber optic carries a larger load and essentially bridges the opening.

Hence, the fiber optics were subjected to harsh testing in these experiments. Since this is considered to be a worst case scenario, the potential for the fibers to perform similarly if not better when properly placed is expected to be high.

Also, due to the harsh environment around the FBG, difficulties in peak wavelength value determination have been highlighted.

Conclusion

Fiber optic sensors, specifically fiber Bragg grating sensors, are attractive for use in internal sensing of fiber reinforced polymers. Further development of their uses and limitations is necessary to further determine their appropriate applicability to the development of structural health monitoring and/or smart structures.

A method of fabricating a composite specimen with an embedded fiber optic sensor using a wet hand lay-up was developed. This method proved to be a repeatable method of fabrication as twelve specimens were fabricated with this method. Further, the fiber optics remained intact for all specimens. The post embedding reflected spectrums were measured and residual strain due to cure was determined. The residual strain values were in close agreement for each specimen type.

The fabrication method was further validated by initial specimen stiffness measurements. Variation between specimens was expected due to the fabrication method as well as the placement of the fiber optic perpendicular to the fiber bundles in the middle layer of the specimen. However, all values were in close agreement.

The embedded FBGs were successful in detecting a drop in stiffness of the specimens due to cyclic loading. Variation existed in the results due to loading differences and specimen variation. It would be difficult to obtain quantitatively comparative results due to the inherent variance of the fabrication method.

The effect of embedding the fiber optic on the reflected spectrum and the reflected spectrums of damaged specimens are qualitatively comparable to those presented in the literature. Further, the quantitative results obtained from the FBGs ability to detect a percentage drop in stiffness, of a fatigue damaged specimen, has not been seen in the literature for an embedded FBG. This is considered to be a promising result in the development of embedded fiber optic sensors in fiber reinforced polymers.

References

1. Measures, R.M. (2001). *Structural monitoring with fiber optic technology*. New York: Academic Press.
2. Baker A., Dutton S. and Kelly D. eds. (2004), *Composite Materials for Aircraft Structures*, AIAA, Virginia, pp. 525-547.
3. Herszberg I. et al. (2007), International Conference on Composite Materials, 16, 6.
4. Beral B. (2007), International Conference on Composite Materials, 16, 24.
5. Arakaki F. and Gonçalves W. (2007), International Conference on Composite Materials, 16, 26.
6. Daniel I. M. & Ishai O. (2006). *Engineering Mechanics of Composite Materials (2nd Ed.)*. New York, NY: Oxford University Press.
7. Swanson S. (1997), *Advanced Composite Materials*, Prentice Hall, New Jersey, pp. 8-18.
8. Strong A.B. (1989), *Fundamentals of Composites Manufacturing: Materials, Methods, and Applications*, Society of Manufacturing Engineers, Michigan, pp. 108-113.
9. Wisnom M.R., Gigliotti M., Ersoy N., Campbell M., & Potter K.D. (2006) Mechanisms generating residual stresses and distortion during manufacture of polymer – matrix composite structures. *Composites: Part A*, 37, 522-529.
10. Reifsnider K.L. (Ed.). (1991). *Composite Materials Series: Vol 4. Fatigue of Composite Materials*. New York NY: Elsevier.
11. Carlson R.L & Kardomateas G.A. (1996). *An Introduction to Fatigue in Metals and Composites*. New York, NY: Chapman & Hall.
12. Kolubinski L., Fawaz Z., Behdinan K. and Poon C. (2007). CASI AERO 2007: 19th Aerospace Structures and Materials Symposium.
13. MIL-HDBK-17-3F (2007). Vol 3, Chapter 5 – Design and Analysis.
14. Harris B. (Ed.). (2003). *Fatigue in Composites; Science and Technology of the fatigue response of fibre-reinforced plastics*. New York, NY: CRC Press.
15. DeCusatis C.M & Sher DeCusatis C.J. (2006). *Fiber Optic Essentials*, Elsevier Inc., New York, pp. 4-10.

16. Hill K.O. & Meltz G. (1997). Fiber Bragg Grating Technology Fundamentals and Overview. *Journal of Lightwave Technology*, 15 (8): 1263-1276.
17. Murayama H. (2007), et.al. International Conference on Composite Materials, 16, 68.
18. Kivshar Y. S. & Agrawal G. P. (2003). *Optical Solitons: From Fiber to Photonic Crystals*. New York, NY: Academic Press.
19. Foote P., Bredne M., Levin K., Papadopolous P., Read I., Signorazzi M., Nilsson L.K., Stubbe R., Claesson A. (2004). Operational Load Monitoring Using Optical Fiber Sensors. In W. Staszewski, C. Boller, G. Tomlinson (Eds.), *Health Monitoring of Aerospace Structures* (pp. 75-124). London, England: John Wiley & Sons Ltd.
20. Gotou T. (2007), et al., Conference on Composite Materials, 16, 64.
21. Kosaka T. (2003), et al., SPIE, 5056, 73.
22. Lee D.C., Lee J.J, Kwon I.B. & Seo D.C. (2001). Monitoring of fatigue damage of composite structures by using embedded intensity-based optical fiber sensors. *Smart Materials and Structures*, 10, 285-292.
23. Güemes J.A., Menendez J.M., Frövel M., Fernandez I. And Pintado J.M. (2001). Experimental analysis of buckling in aircraft skin panels by fibre optic sensors. *Smart Material and Structures*, 10, 490-496.
24. Eum S.H., Kageyama K., Murayama H., Uzawa K., Ohsawa I., Kanai M., Kobayashi S., Igawa H. & Shirai T. (2007). Structural health monitoring using fiber optic distributed sensors for vacuum-assisted resin transfer molding. *Smart Materials and Structures*, 16, 2627-2635.
25. Kosaka T., Osaka K., Nakakita S., & Fukuda T. (2003). Fiber optic strain monitoring of textile GFRP during RTM molding and fatigue tests by using embedded FBG sensors. *Smart Structures and Materials*, 5056, 73-80.
26. Dewynter-Marty V., Ferdinand P., Bocherens E., Carbone R., Beranger H., Bourasseau S. et al. (1998). Embedded fiber Bragg Grating Sensors for Industrial Composite Cure Monitoring. *Journal of Intelligent Material Systems and Structures*. 9: 785-787.

27. Roberts S.S.J. & Davidson R. (1993). Cure and Fabrication Monitoring of Composite Materials with Fiber-Optic Sensors. *Composites Science and Technology*, 49: 265-276.
28. Chehura E., Skordos A.A., Ye C.C., James S.W., Partridge I.K., & Tatam R.P. (2005). Strain development in curing epoxy resin and glass fiber/epoxy composites monitored by fiber Bragg grating sensors in birefringent optical fiber. *Smart Materials and Structures*, 14: 354-362.
29. Guo Z.S., Zhang B. & Du S.Y. (2007). Theoretical and Experimental Studies on Residual Stresses of Advanced Polymer Composites. *Key Engineering Materials Vols.*, 334-335, 37-40.
30. Holl M. and Boyd S. (1993). The effect of embedded fiber optics on the mechanical properties of the composite host material. *SPIE*, 1916, 109-117.
31. Roberts S.S.J. & Davidson R. (1991). Mechanical Properties of Composite Materials Containing Embedded Fibre Optic Sensors. *SPIE Fiber Optic Smart Structures and Skins IV*, 1588, 326-341.
32. Barton E.N., Ogin S.L., Thorne A.M., Reed G.T., & LePage R.H. (2001). Interaction between optical fibre sensors and matrix cracks in cross-ply GRP laminates – part 1: passive optical fibres. *Composites Science and Technology*, 61, 163-169.
33. Guemes J.A. & Menéndez J.M. (2002). Response of Bragg grating fiber-optic sensors when embedded in composite laminates. *Composites Science and Technology*, 62, 959-966.
34. Botsis J., Humbert L., Colpo F., & Giaccari P. (2005). Embedded fiber Bragg grating sensor for internal strain measurements in polymeric materials. *Optics and Lasers in Engineering*, 4, 491-510.
35. Kuang K.S.C., Kenny R., Whelan M.P., Cantwell W.J. & Chalker P.R. (2001). Embedded fibre Bragg grating sensors in advanced composite materials. *Composites Science and Technology*, 61, 1379-1387.
36. Okabe Y., Yashiro S., Tsuji R., Mizutani T. & Takeda N. (2002). Effect of thermal residual stress on the reflection spectrum from fiber Bragg grating sensors embedded in CFRP laminates. *Composites: Part A*, 33, 991-999.

37. Takeda N. (2002). Characterization of microscopic damage in composite laminates and real-time monitoring by embedded optical fiber sensors. *International Journal of Fatigue*, 24, 281-289.
38. Liu T., Fernando G.F., Rao Y.J., Jackson D.A., Zhang L. & Bennion I. (1996). In-site strain measurements in composites during fatigue testing using optical fibre Bragg gratings and a portable CCD detection system. *SPIE*, 2895, 249-257.
39. Shin C.S. & Chiang C.C. (2006). Fatigue damage monitoring in polymeric composites using multiple fiber bragg gratings. *International Journal of Fatigue*, 28, 1315-1321.
40. Shin C.S. & Chiang C.C. (2006). Embedded Fibre Bragg Grating Sensors for Internal Fatigue Damage Monitoring in Polymeric Composites. *Key Engineering Materials*, 321-323, 230-233.
41. Kosaka T., Kurimoto H., Osaka K., Nakai A., Osada T., Hamada H. & Fukuda T. (2004). Strain monitoring of braided composites by using embedded fiber-optic strain sensors. *Advanced Composite Materials*, 13 no. 3-4, 157-170.
42. *Micron Optics Inc*: Company website (2007). Retrieved April 20, 2007, from <http://www.micronoptics.com>.
43. Vishay Micro-Measurements. Tech Note TN-505-4 (2007). Strain Gage Selection: Criteria, Procedures, Recommendations.
44. Dally J. & Riley W. (1991). *Experimental Stress Analysis* (3rd ed). Toronto: McGraw-Hill Inc.
45. Vishay Micro-Measurements. Tech Note TN-508-1 (2007). Fatigue Characteristics of Vishay Micro-Measurements Strain Gages.
46. Vishay Micro-Measurements. Application Note TT-604 (2007). Leadwire Attachment Techniques for Obtaining Maximum Fatigue Life of Strain Gages.
47. Vishay Micro-Measurements. Tech Note TN-502 (2007). Optimizing Strain Gage Excitation Levels.
48. ASTM D 3039. (2006). Standard Test Method for Tensile Properties of Polymer Matrix Composite Materials. USA: ASTM International.
49. Vishay Micro-Measurements. Application Note B-129-8 (2005). Surface Preparation for Strain Gage Bonding.